Available online at www.sciencedirect.com
ScienceDirect
Lithos 96 (2007) 127–150
LITHOS
www.elsevier.com/locate/lithos

Contrasting zircon Hf and O isotopes in the two episodes of Neoproterozoic granitoids in South China: Implications for growth and reworking of continental crust

Yong-Fei Zheng [a,b,*], Shao-Bing Zhang [a], Zi-Fu Zhao [a], Yuan-Bao Wu [a,c], Xianhua Li [d], Zhengxiang Li [e], Fu-Yuan Wu [b]

[a] CAS Key Laboratory of Crust–Mantle Materials and Environments, School of Earth and Space Sciences, University of Science and Technology of China, Hefei 230026, China
[b] State Key Laboratory of Lithosphere Evolution, Institute of Geology and Geophysics, Chinese Academy of Sciences, Beijing 100029, China
[c] Faculty of Earth Sciences, China University of Geosciences, Wuhan 430074, China
[d] CAS Kay Laboratory of Isotope Geochronology and Geochemistry, Guangzhou Institute of Geochemistry, Chinese Academy of Sciences, Guangzhou 510640, China
[e] Tectonics Special Research Centre, School of Earth and Geographical Sciences, The University of Western Australia, Crawley, WA 6009, Australia

Received 12 October 2005; received in revised form 18 September 2006; accepted 24 October 2006
Available online 29 December 2006

Abstract

The genetic links among rift magmatism, crustal growth and water–rock interaction are an important issue about mass and heat transfer between mantle and crust during supercontinent breakup. A combined study of Hf and O isotopes in zircons from Neoproterozoic granitoids in South China provides evidence for growth and reworking of juvenile and ancient crusts with different styles of water–rock interactions along rift tectonic zones. Two generations of the granitoids show contrasting features in both zircon Hf and O isotope compositions, indicating their distinct petrogenesis. The ~825 Ma granitoids exhibit negative $\varepsilon_{Hf}(t)$ values of −3.4±0.8 to −1.6±0.8 with old model Hf ages of 1.81±0.07 to 1.92±0.10 Ga, and high $\delta^{18}O$ values of 8.7 to 10.4‰. These indicate that the source material of granitoid magmas was derived from melting of Paleoproterozoic basement that has the Hf isotope signature similar to the enriched mantle but experienced chemical weathering process before anatexis. Reworking of ancient crust is demonstrated to occur at ~825 Ma in the orogenic collapse zone, with overprinting of subsolidus hydrothermal alteration during magma emplacement. In contrast, the 760–750 Ma bimodal intrusives are characterized by positive $\varepsilon_{Hf}(t)$ values of 3.5±0.8 to 9.9±0.8 with young model Hf ages of 0.94±0.06 to 1.18±0.06 Ga, and both low and high $\delta^{18}O$ values of 4.2 to 6.2‰ relative to 5.3±0.3‰ for the normal mantle zircon. Prompt reworking of juvenile crust is suggested to occur at ~750 Ma in the rifted tectonic zone, with occurrence of supersolidus hydrothermal alteration and local low-^{18}O magmatism during supercontinent breakup. Contributions of the depleted mantle to their magma sources are contrasting in the two episodes of magmatism in association with breakup of the supercontinent Rodinia. While the change in melt source from the crust to the mantle keeps pace with the advance from continental rifting to supercontinent breakup, significant transport of both heat and material from the depleted mantle to the continental crust only occurred along the active rifting zone. In either case, the growth and reworking of continental crust are episodically associated with rift magmatism.

Keywords: Zircon; Hf isotope; O isotope; Neoproterozoic magmatism; South China; Continental growth; Mantle upwelling; Supercontinent breakup

* Corresponding author.
E-mail address: yfzheng@ustc.edu.cn (Y.-F. Zheng).

0024-4937/$ - see front matter © 2006 Elsevier B.V. All rights reserved.
doi:10.1016/j.lithos.2006.10.003

1. Introduction

Growth and reworking of the continental crust in the history of the Earth are of substantial importance in understanding its chemical characteristics and underlying crust–mantle differentiation (Brown and Rushmer, 2005). While subduction-related arc magmatism has contributed juvenile crust to continental accretion (e.g., Rudnick, 1995; Condie and Chomiak, 1996), arc–continent collision and postcollisional collapse are two critical processes to cause intracrustal differentiation and thus to shape the major chemical feature of continental crust (e.g., Wu et al., 2006a). On the other hand, plume-related magmatism can also result in continental growth via either horizontal accretion of oceanic plateau and island basalts or vertical addition of continental flood basalts (e.g., Albarede, 1998; Condie, 2000), regardless of their origin from the core–mantle boundary, or the transition zone or the top of the asthenospheric mantle (Courtillot et al., 2003), and so can melting of subducted oceanic slabs in association with island arc magmatism (e.g., Defant and Drummond, 1990; Yogodzinski et al., 2001). Nevertheless, arc-like patterns of trace element partition in most igneous rocks on the continental crust clearly make reworking of arc-derived rocks the dominant mechanism. With respect to extraction of juvenile crust from the asthenospheric mantle, on the other hand, volcanic rifted margins are also a favorite site for continental growth (Zheng et al., 2006).

Rift magmatism has been found in close association with supercontinent breakup and mantle superwelling (or superplume event as defined by Larson, 1991a,b). Although generation of Proterozoic and Phanerozoic continental crust is predominated by orogenic magmatism in arc–continent collision belts (Rudnick, 1995; Condie and Chomiak, 1996; Wu et al., 2006a), rift magmatism is also an additional way for continental growth along broken up continental margins (Zheng et al., 2006). Heat from a zone of upwelling asthenosphere beneath the continental crust may cause extensive melting of both the subcontinental lithospheric mantle and the mafic lower crust to produce the bimodal igneous rocks of mafic and felsic compositions, respectively (Campbell and Hill, 1988). In association with extensional collapse of collision-thickened orogens (Dewey, 1988), thermal reworking by mantle upwelling may have played a significant role in the formation of intracontinental magmatic provinces (Thompson and Connolly, 1995). Therefore, it is important to know how matter and energy transfer from the mantle to the crust proceeds during rift magmatism with respect to growth and reworking of juvenile and ancient crust.

Zircon is a refractory mineral that forms a highly robust phase in most geological environments and thus is ideal for radiometric dating and geochemical tracing (Hanchar and Hoskin, 2003, and references therein). Zircon U–Pb ages register magmatic episodes related to crustal reworking, whereas zircon model Hf ages can provide a first approximation to timing of crustal extraction from the mantle in the extreme case where its initial Hf isotope composition approaches that of the contemporaneous depleted mantle (Zheng et al., 2006). A combined study of zircon U–Pb age and Hf isotope has the potential to date melt extraction, hence growth of juvenile crust and reworking of ancient crust by melting. If growth occurs shortly before reworking, as may occur at sites of continental and back-arc rifting, then it happened so close in time to the crustal reworking that it is not detectable from the Lu–Hf isotopic systematics. In contrast, if crustal growth occurs significantly before crustal reworking, as may occur at sites of arc–continent and continent–continent collision events, then post-collisional magmatism in these regions should result in its product with considerably older model Hf ages than the U–Pb ages.

Furthermore, bimodal magmatism and high-T water–rock interaction may be developed along rift tectonic zones, with potential incorporation of surface water into magmas via remelting of hydrothermally altered rocks. Therefore, it is necessary to identify these components in coeval igneous rocks that developed along supercontinental margins and thus to constrain the genetic relationship among rift magmatism, juvenile crust growth and surface fluid activity. In addition to its advantage for U–Pb dating, zircon provides high-quality records of Hf and O isotope compositions that can be simultaneously used both in protolith studies and as petrogenetic indicators (Hawkesworth and Kemp, 2006; Kemp et al., 2006; Zhang et al., 2006). This paper presents a combined study of Hf and O isotopes in zircons from Neoproterozoic intrusives along the margins of the Yangtze Craton in South China. The results provide geochemical evidence for growth and reworking of continental crust during arc–continent collision and rift magmatism in association with assembly and breakup of the supercontinent Rodinia.

2. Geological settings and samples

Neoproterozoic igneous rocks of felsic and mafic compositions are widespread around the Yangtze Craton in the South China Block (Fig. 1). Their distribution coincides in general with the distribution of Cryogenian continental rift systems (Wang and Li, 2003). The bimodal igneous rocks can be subdivided into two major

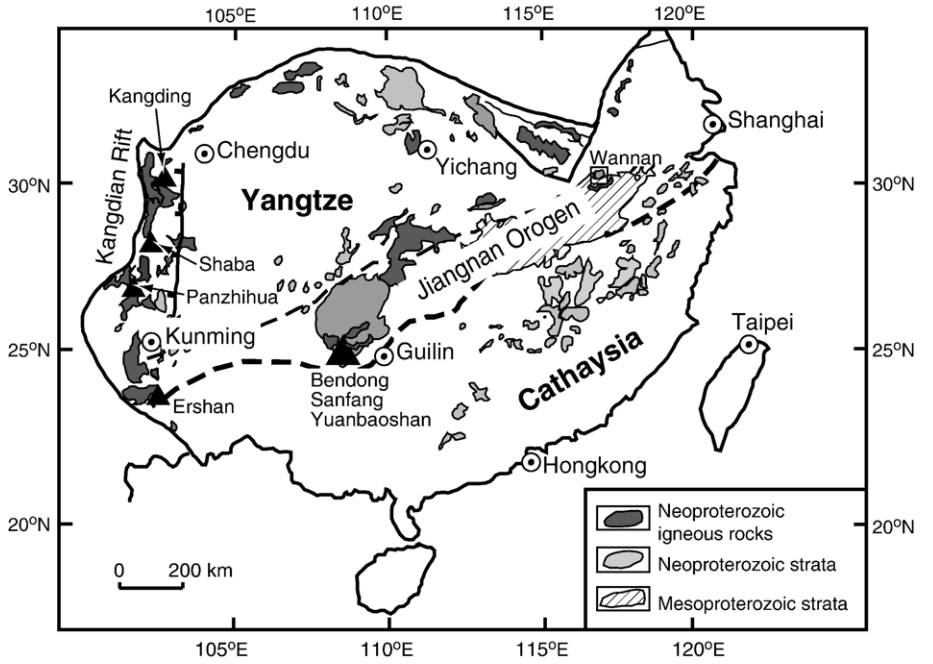

Fig. 1. Sketch map of geology in South China, with the distribution of Neoproterozoic intrusives around the Yangtze Craton. Triangle denotes the sample locality in this study: (1) about 825 Ma granitoids at Bendong, Sanfang and Yuanbaoshan in North Guangxi and at Eshan in Central Yunnan, the western part of the Jiangnan Orogen between the Yangtze and Cathaysia Cratons; (2) about 760–750 Ma bimodal intrusives at Kangding, Shaba and Panzhihua in West Sichuan, along the Kangdian Rift in the western margin of the Yangtze Craton.

associations according to their ages relative to rifting event (Li et al., 2003a,b). The early association, traditionally called the Jinning suite and often overlain unconformably by rift successions, generally has an age range of ca. 830 to 820 Ma and is thus regarded as a pre-rift suite. They occur along the NE-trended Jiangnan Orogen between the Yangtze Craton and the Cathaysia Craton (Li, 1999; Li et al., 1999, 2003a; Wu et al., 2006a), both cratons being assembled during the Grenvillian orogeny (e.g., Charvet et al., 1996; Zhao and Cawood, 1999; Li et al., 2002a; Li and Li, 2003). The late association, traditionally called the Chengjiang suite, often intrudes the rift successions but is in places unconformably overlain by the equivalent of the Ediacaran Doushantuo Formation (Wang and Li, 2003), with an age range of ca. 780 to 740 Ma and thus belongs to a syn-rift suite. They occur in the Kangdian rift belt along the western margin of the Yangtze Craton (Li et al., 2002b, 2003b) and in the Dabie–Sulu orogenic belt along the northern margin of the Yangtze Craton (Zheng et al., 2004, 2006).

This paper focuses on the older pre-rift granitoids from the northern part of the Guangxi Province (hereafter North Guangxi) and the central part of the Yunnan Province (Central Yunnan) in the western part of the Jiangnan Orogen, and the younger syn-rift bimodal intrusives along the Kangdian rift belt in the western part of the Sichuan Province (West Sichuan).

2.1. North Guangxi

Neoproterozoic granitoids outcrop over 1500 km^2 in North Guangxi. They intrude the tightly folded Mesoproterozoic Sibao Group, and are overlain unconformably by Neoproterozoic rift strata of the Danzhou Group. Coarse-grained muscovite leucogranite is the dominant rock type, and is exposed over ~1400 km^2, including the Sanfang batholith (~1000 km^2), the Yuanbaoshan batholith (~300 km^2) and several small plutons and stocks (Fig. 1). Biotite granodiorite (~85 km^2) makes up the remainder of the granitoids in the region, including the Bendong Pluton (~40 km^2) and a few smaller plutons and stocks.

Previous SHRIMP and ID-TIMS zircon U–Pb dating yield concordant ages of 819±9, 826±10 and 824±4 Ma for the Bendong, Sanfang and Yuanbaoshan plutons, respectively (Li, 1999), indicating that these granitoids are essentially coeval at ca. 820–825 Ma. Furthermore, the 819–826 Ma granitoids are closely associated in time and space with the 828±7 Ma mafic and ultramafic intrusions in North Guangxi (Li et al., 1999), constituting the first generation of bimodal intrusives in the pre-rift period.

2.2. Central Yunnan

Neoproterozoic granitoids in Central Yunnan are represented by the Eshan pluton (Fig. 1), which crops out over ~200 km^2 to the south of Eshan County. The pluton intruded Mesoproterozoic metamorphic rocks of the Kunyang Group, and is overlain unconformably by the lower Sinian System sandstones (the Chengjiang Formation) and glacial deposits (the Nantuo Formation). K-feldspar porphyritic granite is the dominant rock type, although quartz diorite and granodiorite are exposed over ~7 km^2 in the northern part of the pluton. Quartz diorite and granodiorite generally display transitional or cross-cutting relationships with the surrounding K-rich granitoids, and diorites occur as enclaves within the K-rich granitoids. Previous SHRIMP zircon U–Pb dating gave a concordant age of 819±8 for a medium-grained K-feldspar porphyritic granite (98KD154) that was collected from the northern part of the pluton for U–Pb zircon analysis (Li et al., 2003a).

2.3. West Sichuan

Neoproterozoic intrusives in West Sichuan are represented by igneous complexes that are distributed almost continuously along the Kangdian Rift (Fig. 1), including granites, granodiorites, tonalites, diorites, gabbros, mafic dykes, and small ultramafic bodies. Some of these igneous complexes intrude the rift succession, but are unconformably overlain by the post-rift platform successions (Li et al., 2003b). The Kangdian Rift is a N–S trending Cryogenian continental rift that was developed on top of a peneplain on strongly deformed, and variably metamorphosed, Mesoproterozoic successions. Radiometric ages for the rift successions (the Suxiong/Kaijianqiao Formations) range from ca. 815±12 Ma (Rb–Sr whole rock isochron) in the middle-lower part to 803±12 Ma (SHRIMP zircon U–Pb) in the middle-upper part of the succession (Li et al., 2002b).

With respect to timing of magma emplacement, five samples from West Sichuan were directly dated by Li et al. (2003b) using the zircon SHRIMP U–Pb technique, yielding ages of 751±10, 752±11 and 752±12 Ma for three samples of granite (98KD70) and gabbro (98KD104 and 98KD111), respectively, and 759±11 and 768±7 Ma for granodiorite (98KD133) and tonalite (98KD36), respectively. It appears that the 751–768 Ma granitoids are closely associated in time and space with the 752±11/12 Ma gabbro in West Sichuan, constituting the second generation of bimodal intrusives in the syn-rift period that were emplaced during the Cryogenian continental rifting in the Yangtze Craton (Li et al., 2003b).

2.4. Samples

Twelve samples of granitoids (including granite, tonalite and granodiorite) and gabbro were used in this study and represent the dominant intrusives that occur in the Cryogenian rifting tectonic zones along the southern and western margins of the Yangtze Craton (Fig. 1). These include granite and granodiorite at Sanfang (90113, 98GX9-1 and 97GX-1), Bendong (98GX16) and Yuanbaoshan (98GX6-5) in North Guangxi, granite at Eshan (98KD154) in Central Yunnan, and granite, tonalite, granodiorite and gabbro at Panzhihua (98KD133 and 98KD139), Shaba (98KD104 and 98KD111) and Kangdian (98KD36 and 98KD70) in West Sichuan.

The Lu–Hf and O isotope analyses were performed on either zircon aliquots of the samples that were directly dated by the SHRIMP U–Pb method (Li et al., 2003a,b), or zircons separated from hand specimens that were used for geochemical analyses (Li, 1999). Individual minerals were further separated by conventional magnetic and heavy-liquid techniques, and then handpicked under binocular microscopes. Although U–Pb ages for the five samples from North Guangxi are not directly available, the same intrusives were dated by either SHRIMP or ID-TIMS technique for their U–Pb ages (Li, 1999). The remaining samples were directly dated by the SHRIMP zircon U–Pb technique, including granite 98KD154 from Eshan in Central Yunnan (Li et al., 2003a), and granitoid and gabbro from West Sichuan (Li et al., 2003b). Tonalite 98KD139 at Panzhihua in West Sichuan was sampled from a locality that is only about 3 km distant from granodiorite 98KD133 at Panzhihua, so that the same U–Pb age of 759±11 Ma can be taken for their magma emplacement.

O isotope analysis was also made on two samples of diabase (97GX-2 and 97GX17) that have a SHRIMP U–Pb age of 828±7 Ma and thus is coeval with the adjacent granitoid at Sanfang (Li et al., 1999), and on a sample of weakly foliated quartz diorite (99KD34) that is about 20 km north-east of Panzhihua with a SHRIMP U–Pb age of 775±8 Ma (Li et al., 2003b).

3. Analytical methods

3.1. Zircon morphology

Zircon grains for the cathodeluminesence (CL) observation were mounted in epoxy resin and polished to expose the grain center. The CL images were obtained

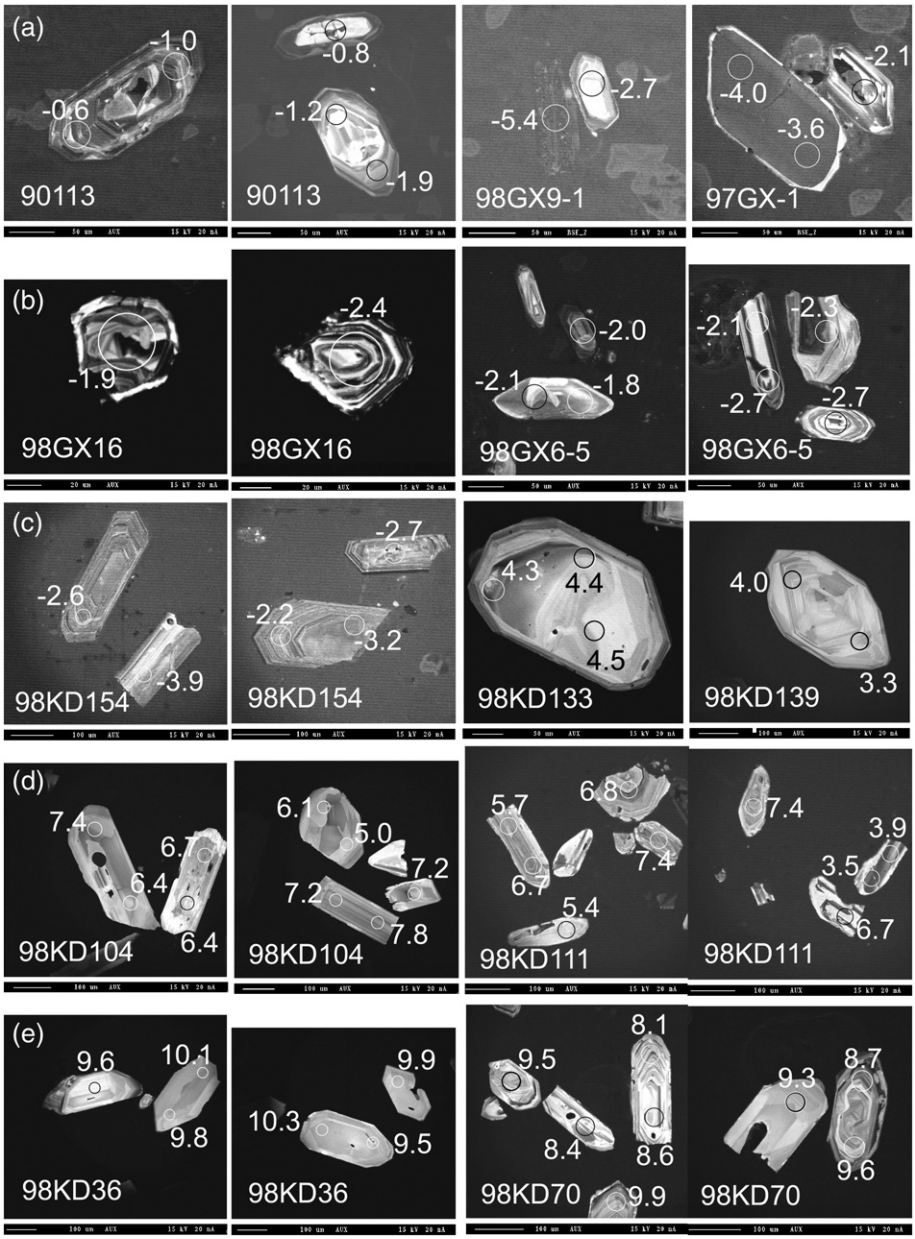

Fig. 2. CL images of zircon grains with initial Hf isotope ratios in $\varepsilon_{Hf}(t)$ for Neoproterozoic intrusives in South China. While some grains show oscillatory zoning typical of igneous origin, occurrence of discontinuous rims around some grains with loss of the zoning indicates overprinting of hydrothermal alteration.

using a microprobe JEOL JXA-8900RL at Institute of Geology and Geophysics in the Chinese Academy of Sciences, Beijing. The working conditions during the CL imaging were at 15 kV. Typical CL pictures are presented in Fig. 2. Morphology and internal structure of zircons are described and interpreted following the conventions of Corfu et al. (2003), Zheng et al. (2004) and Hoskin (2005). Together with their Th/U ratios, igneous zircon is classified into co-magmatically grown zircon and residual zircon (inherited from source rock), and hydrothermal zircon into hydrothermally altered zircon and hydrothermally grown zircon.

3.2. Lu–Hf isotopes

Zircon Hf isotope analysis was carried out *in-situ* using a Geolas-193 laser-ablation microprobe, attached to a Neptune multi-collector ICPMS, at the Institute of

Geology and Geophysics in the Chinese Academy of Sciences, Beijing. Instrumental conditions and data acquisition were comprehensively described by Xu et al. (2004). The laser system delivers a beam of 193 nm UV light from an excimer laser. The laser repetition was operated at 6 to 10 Hz for a higher intensity of signals. A stationary spot was used for the present analyses, with a beam diameter of either 32 μm or 63 μm depending on the size of ablated domains. Both He and Ar carrier gases were used to transport the ablated sample from the laser-ablation cell via a mixing chamber to the ICPMS torch. A signal collection model for one block with 200 cycles, in which one cycle has 0.131 second integration time and bulk time for one measurement lasts about 30 s. Our routine run of zircon 91500 gave a weighted mean $^{176}Hf/^{177}Hf$ ratio of 0.282306±25 (2σ), which is exactly the same as a weighted mean $^{176}Hf/^{177}Hf$ ratio of 0.282306±10 from solution analysis of Woodhead et al. (2004). Therefore, zircon 91500 was used as the reference standard with $^{176}Hf/^{177}Hf$=0.282306 for the final data processing. All the Lu–Hf isotope analysis results are listed in Table 1 (online Appendix A) with the error in 2σ of the mean.

The isobaric interference of ^{176}Lu on ^{176}Hf was corrected by measuring the intensity of the interference-free ^{175}Lu isotope and using a recommended $^{176}Lu/^{175}Lu$ ratio of 0.02655 (Machado and Simonetti, 2001). Similarly, the isobaric interference of ^{176}Yb on ^{176}Hf was corrected by measuring the interference-free ^{172}Yb isotope and using a recommended $^{176}Yb/^{172}Yb$ ratio of 0.5886 (Chu et al., 2002) to calculate $^{176}Hf/^{177}Hf$ ratios. In doing so, the appropriate $^{176}Yb/^{172}Yb$ ratio was determined by successive spiking the solution of JMC 14374 with variable Yb/Hf ratios (Griffin et al., 2000). In order to check the data quality, some of high $^{176}Yb/^{177}Hf$ domains were reanalyzed, together with five standard zircons (91500, TEMORA, CZ3, CN92-1 and FM0411), following the suggestion of Woodhead et al. (2004) but the procedures of Iizuka and Hirata (2005). A mean $^{173}Yb/^{171}Yb$ ratio for the analyzed spot itself was automatically used in the same run to calculate a mean β_{Yb} value; then the ^{176}Yb signal intensity was calculated from the ^{173}Yb signal intensity and the mean β_{Yb} value (Wu et al., 2006b). In terms of the significant differences in $^{176}Yb/^{177}Hf$, $^{176}Lu/^{177}Hf$ and $^{176}Hf/^{177}Hf$ ratios between the five standard zircons, a program was developed to reprocess the previous raw data for the ^{176}Yb–^{176}Lu–^{176}Hf interference corrections. The quality of the reprocessed data is controlled by comparison with the new data on the same domains as the previous analyses and with the reprocessed data for the standard zircons.

Table 2
Oxygen isotope composition of minerals from Neoproterozoic intrusives in South China

Sample no.	Mineral	$\delta^{18}O$ (‰)	Pair	$\Delta^{18}O$ (‰)	T (°C)
North Guangxi					
90113	Zircon	8.76			
Sanfang					
98GX9-1	Quartz	12.15			
Sanfang	K-feldspar	9.25	Qz-Kfs	2.90	240
	Plagioclase	9.22	Qz-Pl	2.93	245
	Zircon	8.98	Qz-Zr	3.17	730
97GX-1	Quartz	11.79			
Sanfang	K-feldspar	9.93	Qz-Kfs	1.86	425
	Plagioclase	9.78	Qz-Pl	2.01	400
	Zircon	8.67	Qz-Zr	3.12	740
97GX-2	Quartz	8.29			
Sanfang	Plagioclase	8.05	Qz-Pl	0.14	>1200
	Biotite	2.46	Qz-Bi	5.83	390
97GX17	Plagioclase	8.84			
Sanfang	Biotite	4.58	Pl-Bi	4.26	295
	Chlorite	6.14	Pl-Chl	2.70	350
98GX16	Quartz	8.58			
Bedong	K-feldspar	6.45	Qz-Kfs	2.13	365
	Plagioclase	6.41	Qz-Pl	2.17	365
	Biotite	1.49	Qz-Bi	7.09	310
	Zircon	9.66	Qz-Zr	−1.08	
98GX6-5	Quartz	13.04			
Yuanbaoshan	K-feldspar	10.47	Qz-Kfs	2.57	285
	Plagioclase	10.37	Qz-Pl	2.67	280
	Tourmaline	10.87	Qz-Tm	2.17	550
	Diopside	10.37	Qz-Di	2.67	735
	Zircon	10.42	Qz-Zr	2.62	840
Central Yunnan					
98KD154	Quartz	9.87			
Eshan	K-feldspar	8.81	Qz-Kfs	1.06	715
	Plagioclase	8.76	Qz-Pl	1.11	700
	Biotite	5.62	Qz-Bi	4.25	535
	Zircon	6.82	Qz-Zr	3.05	755
	Magnetite	3.27	Qz-Mt	6.60	615
West Sichuan					
98KD133	Zircon	6.23			
Panzhihua					
98KD139	Quartz	8.64			
Panzhihua	Plagioclase	6.98	Qz-Pl	1.66	575
	Hornblende	5.57	Qz-Hb	3.07	675
	Biotite	4.07	Qz-Bi	4.57	500
	Zircon	6.21	Qz-Zr	2.43	885
99KD34	Quartz	7.82			
Panzhihua	Plagioclase	5.57	Qz-Pl	2.25	425
	Hornblende	4.83	Qz-Hb	2.99	690
	Epidote	4.23	Qz-Bi	3.59	470
	Chloride	4.08	Qz-Chl	3.74	515
	Zircon	5.27	Qz-Zr	2.55	855
98KD104	Quartz	8.66			
Shaba	Plagioclase	5.58	Qz-Pl	3.08	290
	Diopside	4.35	Qz-Di	4.31	480
	Zircon	4.21	Qz-Zr	4.45	550

Table 2 (*continued*)

Sample no.	Mineral	$\delta^{18}O$ (‰)	Pair	$\Delta^{18}O$ (‰)	T (°C)
	Magnetite	−0.17	Qz-Mt	8.73	480
98KD111	Quartz	8.36			
Shaba	K-feldspar	3.64	Qz-Kfs	4.72	<200
	Plagioclase	3.54	Qz-Pl	4.82	<200
	Hornblende	2.96	Qz-Hb	5.40	395
	Zircon	4.20	Qz-Zr	4.16	585
	Epidote	1.48	Qz-Ep	6.88	210
98KD36	Quartz	8.98			
Kangding	Plagioclase	6.61	Qz-Pl	2.37	400
	Muscovite	2.91	Qz-Mus	6.07	225
	Hornblende	4.32	Qz-Hb	4.66	465
	Zircon	5.45	Qz-Zr	3.53	670
98KD70	Quartz	6.99			
Kangding	K-feldspar	5.68	Qz-Kfs	1.31	600
	Plagioclase	5.51	Qz-Pl	1.48	635
	Hornblende	3.79	Qz-Hb	3.20	655
	Titanite	2.78	Qz-Tt	4.21	645
	Zircon	4.35	Qz-Zr	2.64	835
	Biotite	2.16	Qz-Bi	4.83	475
	Epidote	2.69	Qz-Ep	4.30	390
	Magnetite	0.04	Qz-Mt	6.95	590

Notes: (1) Temperature estimates based on the fractionation relations calibrated by Zheng (1991, 1993a,b); (2) An content of plagioclase is taken to be 10% for granitoids in Guangxi and Yunnan, but 30% for bimodal intrusives in Sichuan and mafic dykes in Guangxi.

Initial $^{176}Hf/^{177}Hf$ ratios are calculated with the reference to the chondritic reservoir (CHUR) at the time of zircon growth from magmas and by using the U–Pb ages that can clearly define the timing of magmatism for the zircons of interest. $\varepsilon_{Hf}(t)$ values are defined to denote the 0.1‰ difference between the sample and the chondritic reservoir at the time of magma crystallization. We have adopted a decay constant for ^{176}Lu of 1.865×10^{-11} yr^{-1} (Scherer et al., 2001), and the chondritic ratios of $^{176}Hf/^{177}Hf$ (=0.282772) and $^{176}Lu/^{177}Hf$ (=0.0332) as derived by Blichert-Toft and Albarede (1997). These values are reported relative to $^{176}Hf/^{177}Hf$=0.282163 for the JMC475 standard. Single-stage "mantle" model Hf ages (T_{DM1}) are calculated using the measured $^{176}Lu/^{177}Hf$ ratios when their $\varepsilon_{Hf}(t)$ values are positive, referred to a model depleted mantle with a present-day $^{176}Hf/^{177}Hf$=0.28325, similar to that of average MORB (Nowell et al., 1998) and $^{176}Lu/^{177}Hf$=0.0384 (Griffin et al., 2000); this is similar, though not identical, to the depleted mantle (DM) curve defined by juvenile rocks through time (Vervoort and Blichert-Toft, 1999). For those zircons that have negative $\varepsilon_{Hf}(t)$ values, we calculate two-stage "crustal" model Hf ages (T_{DM2}) for their source materials assuming a $^{176}Lu/^{177}Hf$ ratio of 0.015 for the average continental crust (Griffin et al., 2002). Errors in both $\varepsilon_{Hf}(t)$ and T_{DM} values are calculated on the basis of analytical errors alone, but much bigger and poorly constrained errors could be associated with the model Hf ages because of errors with the reference model.

3.3. O isotopes

Oxygen isotope analysis of mineral separates was conducted by the laser fluorination technique using a 25W MIR-10 CO_2 laser at Laboratory for Chemical Geodynamics, University of Science and Technology of China in Hefei. O_2 was directly transferred to the Finnigan Delta+mass spectrometer for the measurement of $^{18}O/^{16}O$ and $^{17}O/^{16}O$ ratios (Sharp, 1990; Zheng et al., 2002). O isotope data are reported as parts per thousand differences (‰) from the reference standard VSMOW in the $\delta^{18}O$ notation. Two reference minerals were used: $\delta^{18}O$=5.8‰ for garnet UWG-2 (Valley et al., 1995), and $\delta^{18}O$=10.0‰ for zircon 91500 (Zheng et al., 2004). Each mineral was analyzed twice. Reproducibilities for repeat measurements of each standard and our samples on a given day were better than ±0.1‰ (1σ) for $\delta^{18}O$. All the O isotope analysis results are listed in Table 2.

Mineral-pair O isotopic temperatures are calculated using the fractionation curves of Zheng (1991, 1993a,b), assuming preservation of isotope equilibration at the scale of sample measurement. Judgment and interpretation of O isotope equilibrium or disequilibrium between coexisting minerals are based on measured fractionation values and resultant sequence of O isotope temperatures in combination with rates of O diffusion in concerned minerals and corresponding sequence of closure temperatures (Giletti, 1986; Zheng and Fu, 1998; Zhao et al., 2004a).

4. Zircon morphology

Zircons in three granitoid samples (90113, 97GX-1 and 98GX9-1) from Sanfang in North Guangxi are subhedral and short prismatic. They range from 50 to 200 μm in length, and have length/width ratios of about 1.5:1 to 3:1. As shown in Fig. 2a, CL imaging reveals that some grains have clear oscillatory zoning, which is typical for magmatic zircon. Whereas the others just show weak zoning, patched zoning and cloudy zoning, and a few of them show resorption structures; discontinuous rims occur around some grains with loss of the zoning of magmatic origin, indicating that the magmatic zircons experienced hydrothermal alteration. A few grains of zircon from leucogranite 90113 have inherited highly luminescent cores.

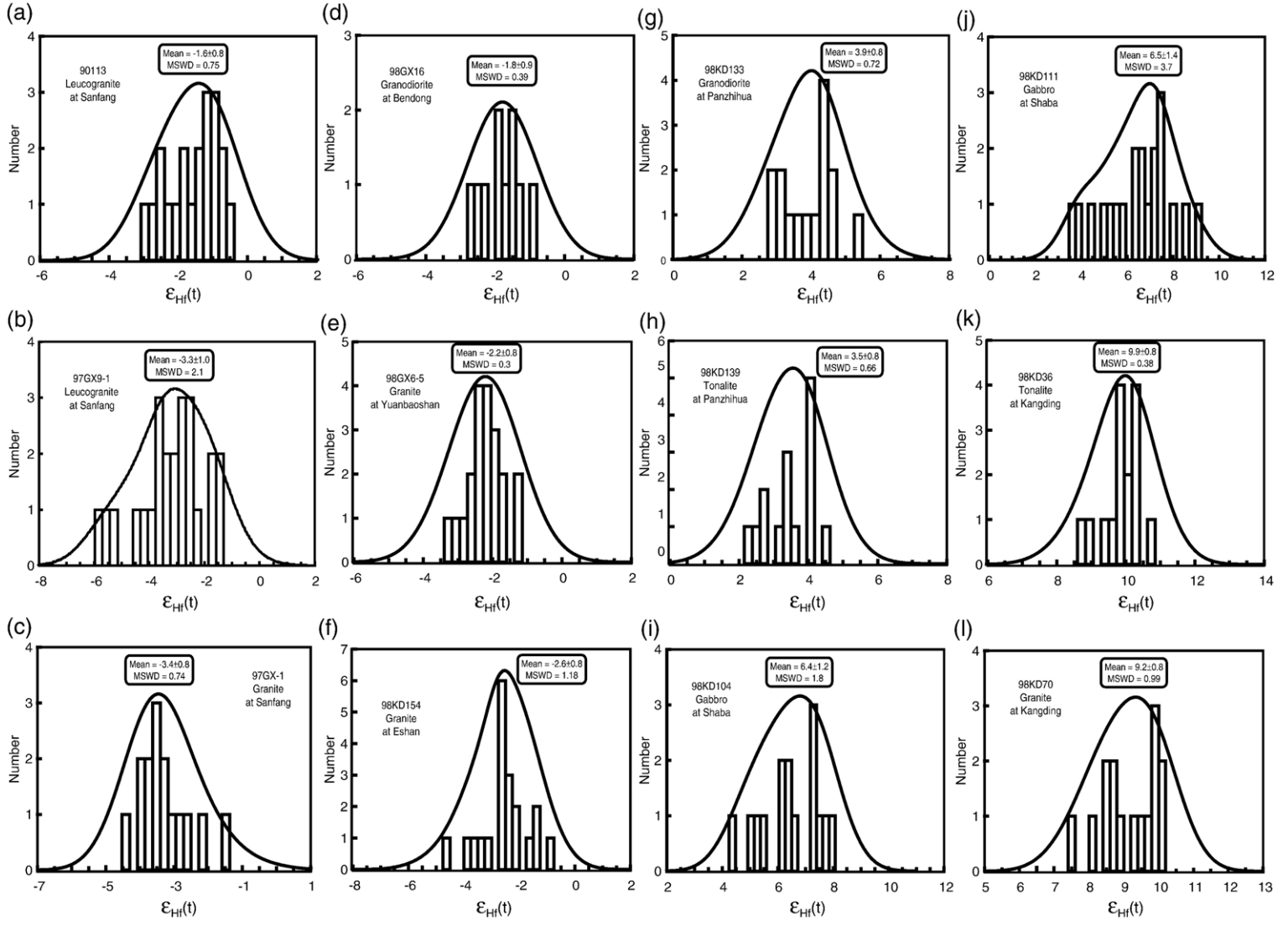

Fig. 3. Histogram of initial Hf isotope ratios for Neoproterozoic intrusives in South China. The ~825 Ma granitoids from the western part of the Jiangnan Orogen exhibit negative $\varepsilon_{Hf}(t)$ values of -3.4 ± 0.8 to -1.6 ± 0.8, whereas the 760–750 Ma bimodal intrusives in the Kangdian Rift are characterized by positive $\varepsilon_{Hf}(t)$ values of 3.5 ± 0.8 to 9.9 ± 0.8.

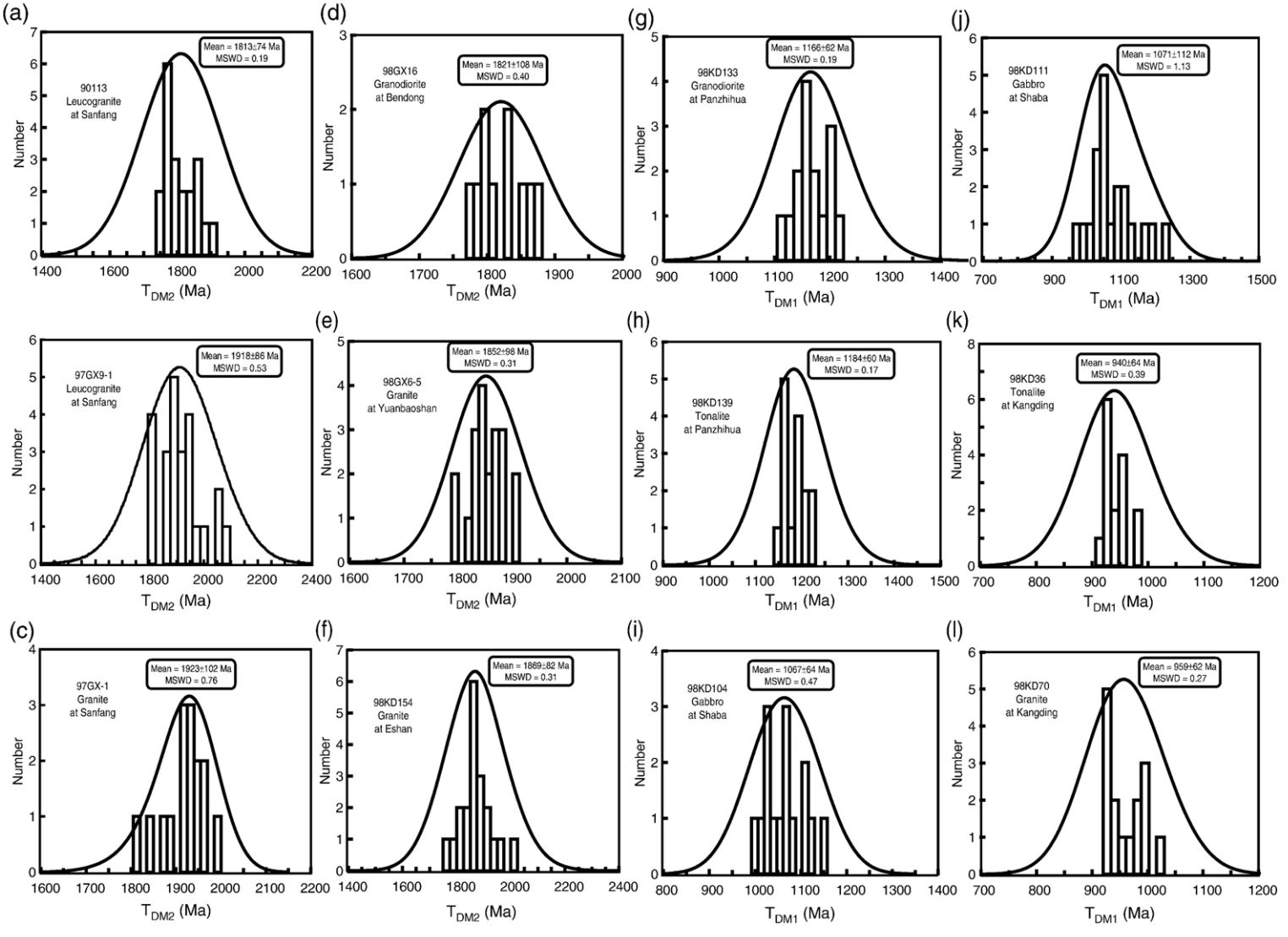

Fig. 4. Histogram of model Hf ages for Neoproterozoic intrusives in South China. The ~825 Ma granitoids from the western part of the Jiangnan Orogen have old model Hf ages of 1.81±0.07 to 1.92±0.10 Ga, whereas the 760–750 Ma bimodal intrusives in the Kangdian Rift show young model Hf ages of 0.94±0.06 to 1.18±0.06 Ga.

Zircons in granodiorite 98GX16 from Bendong and granite 98GX6-5 from Yuanbaoshan are relatively transparent and colorless, and are equant to prismatic in shape. The lengths of these grains range from 40 to 200 μm, with length/width ratios of 1:1 to 4:1. Most of them have clear oscillatory zoning (Fig. 2b), which is typical for magmatic zircon. A few of the grains from granodiorite 98GX16 show embayed boundaries, and some of the grains from granite 98GX6-5 exhibit relict zoning, suggesting that the primary structure of magmatic zoning was modified by hydrothermal alteration.

Zircons in granite 98KD154 from Eshan in Central Yunnan are colorless, transparent and long prismatic grains. The lengths of these grains range from 150 to 300 μm, with length/width ratios of 2:1 to 4:1. They show euhedral shape. CL imaging reveals they have clear concentric oscillatory zoning (Fig. 2c), which forms in zircon during crystallization from a melt. A few of the grains exhibit patched zoning, probably also relevant to post-magmatic alteration.

Zircons in three samples of granitoid (98KD133, 98KD139 and 98KD70) from Panzhihua and Kangding in West Sichuan are colorless, clear and long prismatic grains. All the grains are euhedral in shape. Most of them show clear oscillatory zoning or sector zoning in CL images (Fig. 2c and e), which is typical for magmatic zircon.

Zircons from tonalite 98KD36 are also colorless, clear and long prismatic grains, with euhedral shape. As shown in Fig. 2e, CL imaging reveals that most zircon grains have little or no internal zonation, and a few of them show resorption structures. Therefore, these zircons may be of magmatic origin, but suffered the effect of hydrothermal alteration.

Zircons from gabbro 98KD104 from Shaba are colorless, translucent and short prismatic grains. Crystal lengths range from 100 to 350 μm, with ratios of length to width ranging from 1:1 to 2.5:1. Most of them show clear oscillatory or planar zoning (Fig. 2d), indicating a magmatic origin. Oscillatory zoning fades progressively until an almost homogeneous, highly luminescent rim appears; the inner boundary of the rim is irregular, and impinges on the original oscillatory zoning. These suggest that the rims were of magmatic origin but experienced hydrothermal alteration.

Zircons from gabbro 98KD111 from Shaba are colorless, transparent, short to long prismatic grains. The lengths of these grains range from 50 to 250 μm, with length/width ratios ranging from 1:1 to 4:1. Some of them are subhedral to euhedral, with clear oscillatory zoning (Fig. 2d), which usually forms in magmatic

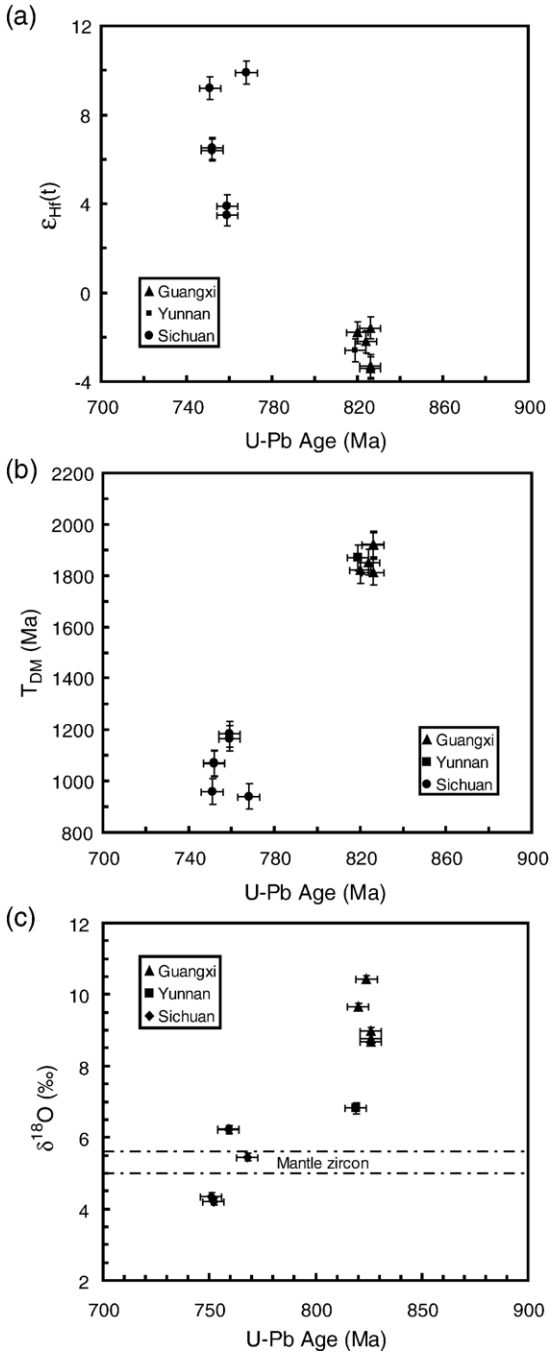

Fig. 5. Relationships of zircon U–Pb age to initial Hf isotope ratio, model Hf age and O isotope composition for Neoproterozoic intrusives in South China. The ~825 Ma granitoids from the Jiangnan Orogen are characterized by high $\delta^{18}O$ values of 8.7 to 10.4‰, whereas the 760–750 Ma bimodal intrusives in the Kangdian Rift show both low and high $\delta^{18}O$ values of 4.2 to 6.2‰ relative to 5.3±0.3‰ for the normal mantle zircon.

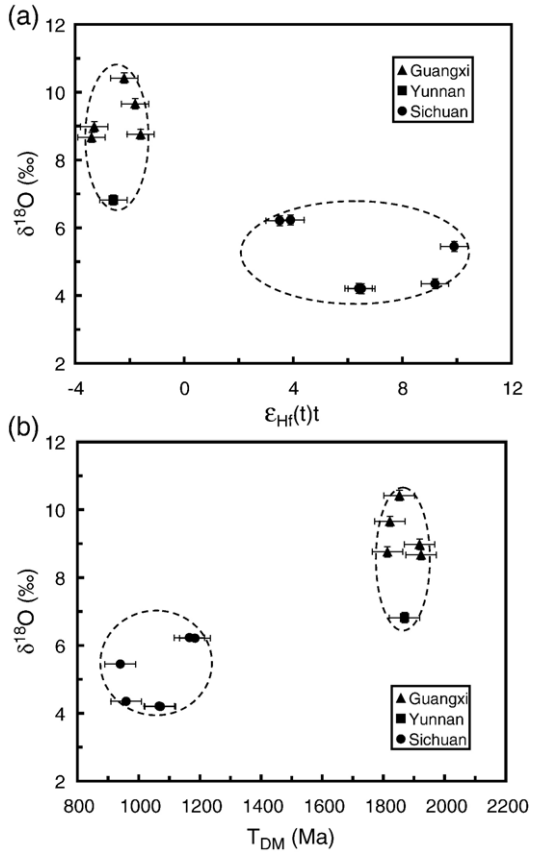

Fig. 6. Relationship of zircon O isotope composition to initial Hf isotope ratio and model Hf age for Neoproterozoic intrusives in South China. There are different mechanisms to determine changes in zircon Hf and O isotopes. While mineral O isotopes are sensitive to supracrustal processes, zircon Hf isotopes are dictated by the Hf budget in the magma source between mantle-derived and crust-derived materials that have contrasting Hf concentrations and isotopic compositions.

environments. The others are subhedral, and show resorption structures with weakly zoning, no zoning or curved zoning, which are interpreted as magmatic grains that experienced hydrothermal alteration.

5. Contrasting signatures of zircon Hf and O isotopes in the two episodes of granitoids

The Lu–Hf isotope data for the zircons are shown in Figs. 3 and 4 as histograms of $\varepsilon_{Hf}(t)$ values and model Hf ages as either T_{DM1} when $\varepsilon_{Hf}(t)>0$ or T_{DM2} when $\varepsilon_{Hf}(t)<0$. Fig. 5 illustrates the relationship of zircon U–Pb ages to $\varepsilon_{Hf}(t)$ values, T_{DM} ages and $\delta^{18}O$ values, Fig. 6 shows the relationship of zircon $\delta^{18}O$ value to $\varepsilon_{Hf}(t)$ values and T_{DM} ages, and Fig. 7 depicts the relationship of O isotope fractionation between quartz, plagioclase and zircon $\delta^{18}O$ values. Table 3 presents a summary of coherent U–Pb, Lu–Hf and O isotope data for the zircon of different ages.

The advantage of LAM-MC-ICPMS *in-situ* analysis is its capability to reveal both intergrain and intragrain heterogeneities in zircon Hf isotopes. The present study of Neoproterozoic igneous rocks shows that within the single granitic samples, there commonly are different zircon populations (based on morphology and CL imaging), and Hf isotope variations among these populations are common. The internal variations of Hf isotopic composition are common for the microscale analyses, with less common isotopic zoning within single zircon grains (e.g., Griffin et al., 2002; Zheng et al., 2005, 2006; Belousova et al., 2006; Zhang et al., 2006). The Hf isotopic heterogeneity can be caused by magma mixing, crustal contamination or source mixing, with insufficient digestion of xenocrystic zircon in

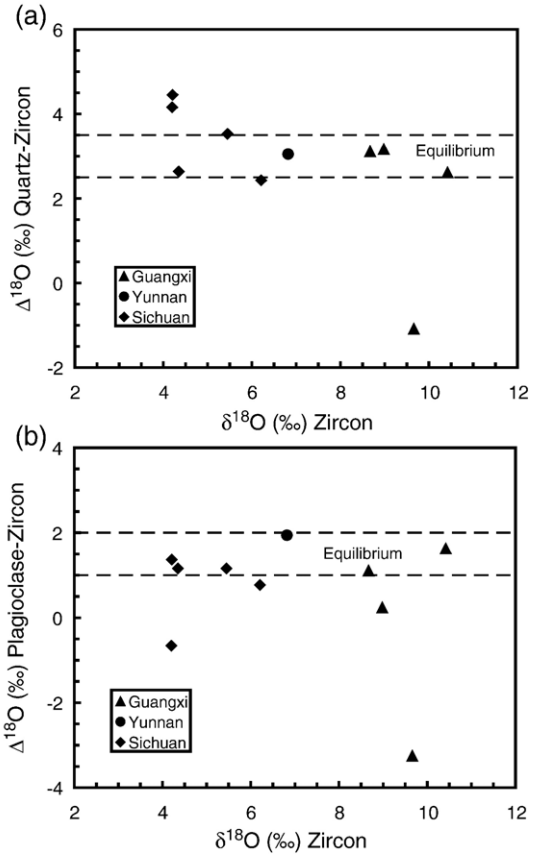

Fig. 7. Plots of O isotope fractionations between quartz or plagioclase and zircon versus the $\delta^{18}O$ values of zircon in Neoproterozoic intrusives in South China. Dashed lines denote the limits of equilibrium fractionation between mineral and zircon, and the samples beyond the two lines are out of isotopic equilibrium. The judgment of equilibrium or disequilibrium fractionations is based on the calibrations of Zheng (1991, 1993a,b).

Table 3
Summary of zircon U–Pb, Lu–Hf and O isotope systematics in Neoproterozoic intrusives from South China

Sample number	Host rock	Locality	U–Pb age			Lu–Hf isotope			Sm–Nd isotope[$]		$\delta^{18}O$
			Method	t (Ma)	Ref. #	$\varepsilon_{Hf}(t)$	T_{DM1} (Ma)	T_{DM2} (Ma)	$\varepsilon_{Nd}(t)$	Ref. #	(‰)
North Guangxi											
90113	Leucogranite	Sanfang	SHRIMP	826±13*	[1]	−1.6±0.8		1813±74			8.76
98GX9-1	Leucogranite	Sanfang	SHRIMP	826±13*	[1]	−3.3±1.0		1918±86	−8.4	[3]	8.98
97GX-1	Granite	Sanfang	SHRIMP	826±13*	[1]	−3.4±0.8		1923±102	−9.0	[3]	8.67
97GX-2	Diabase	Sanfang	SHRIMP	828±7	[2]				−4.2	[5]	8.05 (Pl)
97GX17	Diabase	Sanfang	SHRIMP	828±7	[2]						8.84 (Pl)
98GX16	Granodiorite	Bendong	SHRIMP	820±18*	[1]	−1.8±0.9		1821±108	−5.1	[3]	9.66
98GX6-5	Granite	Yuanbaoshan	ID-TIMS	824±4*	[1]	−2.2±0.8		1852±98	−6.0	[3]	10.42
98GX4-2	Diabase	Yuanbaoshan							−3.4	[5]	
Central Yunnan											
98KD154	Granite	Eshan	SHRIMP	819±8	[3]	−2.6±0.8		1869±82	−8.7	[3]	6.82
West Sichuan											
98KD133	Granodiorite	Panzhihua	SHRIMP	759±11	[4]	3.9±0.8	1166±62				6.23
98KD139	Tonalite	Panzhihua	SHRIMP	759±11*	[4]	3.5±0.8	1184±60				6.21
99KD34	Quartz diorite	Panzhihua	SHRIMP	775±8	[4]						5.27
98KD104	Gabbro	Shaba	SHRIMP	752±12	[4]	6.4±1.2	1067±64		3.1	[4]	4.21
98KD111	Gabbro	Shaba	SHRIMP	752±11	[4]	6.5±1.4	1071±112		3.4	[4]	4.20
98KD36	Tonalite	Kangding	SHRIMP	768±7	[4]	9.9±0.8	940±64				5.45
98KD70	Granite	Kangding	SHRIMP	751±10	[4]	9.2±0.8	959±62				4.35

Notes: superscript *denotes the U–Pb age on the same intrusive; # denotes the following references for U–Pb age: [1] Li XH et al. (1999), [2] Li XH et al. (1999), [3] Li XH et al. (2003a,b), [4] Li XH et al. (2003a,b), [5] Ge et al. (2001); superscript [$] denotes the whole-rock data.

evolved melts. Micro-domain U–Pb dating by means of SIMS or LA-ICPMS techniques also shows the significant inheritance of Pb isotopes in zircon from both I- and S-type granites (e.g., Williams, 1992; Keay et al., 1999; Zhao et al., 2004b, 2007; Huang et al., 2006; Wu et al., 2006a).

The presence of inherited radiogenic Pb in the zircons from the granitoids in North Guangxi is suggested by several $^{207}Pb/^{206}Pb$ ages of 915±18 to 1691±11 Ma (Li, 1999). This indicates the survival of old zircon relicts during the Neoproterozoic magmatism. In fact, zircon can survive episodes of partial melting under conditions of migmatization and magmatism (e.g., Watson, 1996). As a result, zircon U–Pb, Lu–Hf and O isotopic systems can variably be reset in the processes of partial melting, depending on protolith nature, temperature, duration and fluid availability. A statistical treatment with the error analyses is used to obtain weighted means of the calculated $\varepsilon_{Hf}(t)$ values and model Hf ages from the measured Hf isotope data (Figs. 3 and 4, and Table 3). This could bring about simplification of the Lu–Hf isotopic system in the individual samples, but the basic features of these data are generalized without significant bias for the purpose of discussing the igneous petrogenesis and crustal evolution.

As depicted in Figs. 5 and 6, the Lu–Hf and O isotope compositions of zircons from the Neoproterozoic granitoids can generally be divided into two groups according to their U–Pb ages. It appears that there are different clusters between $\delta^{18}O$, $\varepsilon_{Hf}(t)$ and model Hf age (T_{DM1} or T_{DM2}) for the two episodes of igneous rocks. Because there are different mechanisms to change the Lu–Hf and O isotope systematics of zircon, the different clusters indicate remarkable difference in the nature of magma sources, with contrasting Hf budgets between crust and mantle for the intrusives of different ages (Fig. 6). In particular, the occurrence of low $\delta^{18}O$ zircons in the ~750 Ma bimodal intrusives from the Kangdian Rift suggests an active rifting setting, where short-term recycling of supracrustal material would be favored to result in remelting and re-emplacement of juvenile igneous rocks (Zheng et al., 2004, 2006).

The zircons of ca. 760–750 Ma ages for the bimodal intrusives in the Kangdian Rift have consistently positive $\varepsilon_{Hf}(t)$ values of 3.5±0.8 to 9.9±0.8, young T_{DM1} ages of 0.94±0.06 to 1.18±0.06 Ga with a weighted mean of 1.07±0.11 Ga (Fig. 8a), and low $\delta^{18}O$ values of 4.2 to 6.2‰ (Table 2). As illustrated in Fig. 9, the positive $\varepsilon_{Hf}(t)$ values close to those of the depleted mantle at the time of zircon crystallization indicate that the bimodal magmas were derived from melting of juvenile, rather

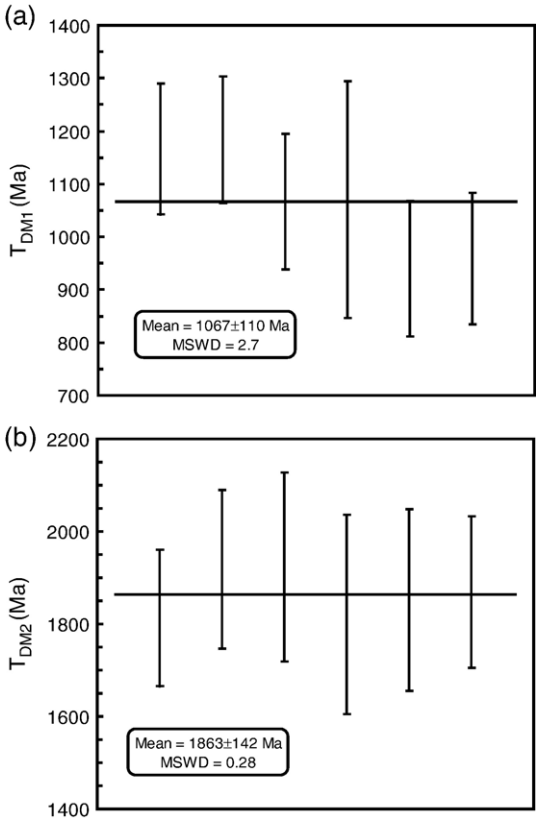

Fig. 8. Weighted mean of model Hf ages for zircons from Neoproterozoic intrusives in South China. (a) The zircons of ca. 760~750 Ma ages for bimodal intrusives in the Kangdian Rift have consistently young T_{DM1} ages of 1.07±0.11 Ga with positive $\varepsilon_{Hf}(t)$ values of 3.5±0.8 to 9.9±0.8; (b) the zircons of ~825 Ma ages for granitoids in the Jiangnan Orogen mostly have older T_{DM2} ages of 1.86±0.14 Ga with negative $\varepsilon_{Hf}(t_1)$ values of −3.4±0.8 to −1.6±0.8.

than ancient, crustal rocks (Zheng et al., 2006). The model T_{DM1} ages of this group are mostly about 0.2 to 0.4 Ga older than their crystallization ages, indicating derivation from juvenile sources that are predominated by magmas extracted from the depleted mantle (Wu et al., 2006a; Zheng et al., 2006). Assuming the $\delta^{18}O$ values of 5.3±0.3 for the normal mantle zircons (Valley et al., 1998), $\delta^{18}O$ values of 5.5 to 6.2‰ for the three samples of granitoid suggest crustal contamination during magmatism, whereas $\delta^{18}O$ values of 4.2 to 4.4‰ for the other three samples of gabbro and granite suggest zircon crystallization from low-^{18}O magmas (Valley et al., 1994; Valley, 2003; Zheng et al., 2004). In either case, the mantle-close $\delta^{18}O$ values of 4.2 to 6.2‰ preclude a significant input by sedimentary component into the magmas from which the zircons crystallized.

In contrast, the zircons of ~825 Ma ages for the granitoids from the Jiangnan Orogen mostly have weakly negative $\varepsilon_{Hf}(t_1)$ values of −3.4±0.8 to −1.6±0.8, older T_{DM2} ages of 1.81±0.07 to 1.92±0.10 Ga with a weighted mean of 1.86±0.14 Ga (Fig. 8b), and high $\delta^{18}O$ values of 6.8 to 10.4‰ (Table 2). The negative $\varepsilon_{Hf}(t)$ values suggest that the granitoid magmas were derived from melting of ancient, rather than juvenile, crustal rocks (Zheng et al., 2006). The model T_{DM2} ages of the second group are mostly about 1.0 to 1.1 Ga older than their crystallization ages, suggesting a possible origin of their parental magmas from the Paleoproterozoic basement. Like contemporaneous granodiorites in South Anhui in the eastern part of the Jiangnan Orogen (Wu et al., 2006a), the high $\delta^{18}O$ values indicated that the pre-rift granitoids were derived from a crustal source that had experienced low-T alteration or chemical weathering processes.

The maximum T_{DM2} ages of 2.05 to 2.07 Ga with the lowest $\varepsilon_{Hf}(t)$ values of −5.7 to −5.4 are obtained for granite 98GX9-1 at Sanfang in North Guangxi (Table 1). This indicates that the continental crust older than about 2.1 Ga, if involved, did not survive the granitic magmatism at ~825 Ma. The two $^{207}Pb/^{206}Pb$ ages of

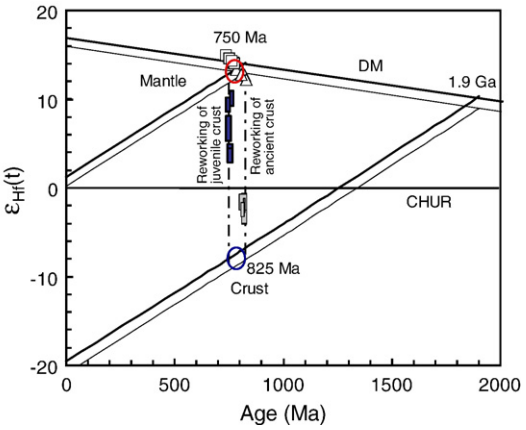

Fig. 9. Diagram of Hf isotope evolution in the zircon from Neoproterozoic intrusives in South China. The ~825 Ma igneous rocks formed by "reworking of ancient crust" that was primarily extracted from the depleted mantle at about 1.9±0.1 Ga. The ~750 Ma igneous rocks formed by prompt "reworking of juvenile crust" with incorporating small amounts of sedimentary component into magma sources. Open triangles denote the protolith of orthogneiss from Port Morvan and Jospinet within the Cadomian Orogen in northwest France (data after Samson et al., 2004), and open squares denote the plagiogranites associated with the Tasriwine ophiolite from the Anti-Atlas orogen in Morocco (Samson et al., 2004). Thick line denotes the evolution of depleted mantle (DM) with a present-day $^{176}Hf/^{177}Hf=0.28325$ and $^{176}Lu/^{177}Hf=0.0384$ (Griffin et al., 2000), and thin lines denotes the evolution of depleted mantle that is drawn by using $\varepsilon_{Hf}(t)=16$ at $t=0$ Ma for MORB at present (Nowell et al., 1998) and $\varepsilon_{Hf}(t)=6$ at $t=2.7$ Ga (Corfu and Noble, 1992; Vervoort et al., 1999). The corresponding lines of crustal extraction are calculated by assuming the $^{176}Lu/^{177}Hf$ ratio of 0.015 for the averaged continental crust.

1092±30 and 1691±11 Ma are dated by Li (1999) for granite from the same pluton, suggesting the survival of Paleoproterozoic zircon relicts but significant resetting by the Neoproterozoic magmatism. If the mean T_{DM2} age of 1.86±0.14 Ga is assumed to be the timing of crustal extraction from the depleted mantle for formation of the Paleoproterozoic basement (Fig. 8b), a crustal member can be proposed with a $^{176}Lu/^{177}Hf$ ratio of 0.015 from ca. ~1.9 Ga to ~825 Ma (the line labeled "reworking of ancient crust" in Fig. 9). In addition to extensional collapse to result in melting of ancient crust (Thompson and Connolly, 1995), a thermal pulse by mantle upwelling may be an efficient mechanism for rejuvenation of lithospheric keel along preexisting orogenic belt.

Some of the samples show the regular sequence of O isotope temperatures from quartz–mineral fractionations (for instance, granite 98GX6-5 at Yuanbaoshan and granite 98KD70 at Kangding in Table 2), in concordance with the difference in rates of O diffusion between these minerals (Zheng and Fu, 1998). This suggests preservation of isotope equilibria under conditions of slow cooling during magma emplacement. On the other hand, some of the samples show disequilibrium O isotope fractionations between quartz and minerals (Table 2 and Fig. 7). For example, two quartz–feldspar pairs from granite 98KD154 gave consistent but higher temperatures of 700 to 715 °C than 615 °C from a quartz–magnetite pair, suggesting possible resetting by post-magmatic alteration because feldspars have much faster rates of O diffusion than magnetite (Giletti, 1986). Post-magmatic alteration is also evident from a disequilibrium fractionation of 0.14‰ between quartz and plagioclase for diabase 97GX-2 and the occurrence of chlorite in diabase 97GX17. The zircon CL imaging also shows that the magmatic zoning was modified to different degrees by hydrothermal alteration (Fig. 2). Nevertheless, the occurrence of chlorite in quartz diorite 99KD34 does not influence the sequence of O isotope temperatures that are generally consistent with the sequence of the closure temperatures of O diffusion in these minerals during slow cooling. Moreover, quartz–biotite (sometimes muscovite) temperatures are lower than quartz–feldspar temperatures, similar to those observed for some of the granodiorites in South Anhui (Wu et al., 2006a). This is incompatible with the closure sequence of O diffusion in biotite and feldspars (Giletti, 1986; Zheng and Fu, 1998) and thus suggests preferential resetting of O isotopes in the biotite relative to the feldspars due to subsolidus alteration by internally derived fluids during magma emplacement.

In contrast, a negative fractionation value of −1.1‰ between quartz and zircon is observed for granodiorite 98GX16 from North Guangxi (Table 2). This indicates significant involvement of an exotic fluid that efficiently exchanged O isotopes with quartz and other minerals under high-T subsolidus conditions during magma emplacement, but it did not change the zircon $\delta^{18}O$ value. Low $\delta^{18}O$ values of 4.2 to 4.4‰ were observed for zircons from gabbro 98KD104 and 98K111 as well as granite 98KD70 in West Sichuan (Table 2), clearly demonstrating that low-^{18}O bimodal magmatism in association with high-T supersolidus water–rock interaction occurred at about 750 Ma (Zheng et al., 2004, 2006). Nevertheless, a zircon $\delta^{18}O$ value of 5.3‰, typical of the mantle zircon $\delta^{18}O$ values, was obtained for quartz diorite 99KD34 at Panzhihua. This indicates that the effect of supersolidus hydrothermal alteration was not significant in this episode of magmatism at 775±8 Ma.

The highest $\varepsilon_{Hf}(t)$ values of 9.2±0.8 to 9.9±0.8 are associated with the youngest T_{DM1} ages of 0.94±0.06 to 0.96±0.06 Ga for the Kangding granitoids in the Kangdian Rift (Table 1), indicating a predominant contribution of juvenile crust to the granitoid source during the ca. 760–750 Ma magmatism. In particular, a low $\delta^{18}O$ value of 4.35‰ occurs in the zircons of the 751±10 Ma granite (Table 3). Furthermore, less high $\varepsilon_{Hf}(t)$ values of 6.4±1.2 to 6.5±1.4 are correlated with less young T_{DM1} ages of 1.07±0.06 to 1.07±0.11 Ga and low $\delta^{18}O$ values of 4.2‰ for the Shaba gabbro of ~750 Ma ages (Table 1), suggesting increased proportions of the supracrustal contribution. It is possible that the juvenile crust would firstly be modified by high-T hydrothermal alteration and then was assimilated by the gabbroic magma during its emplacement at ~750 Ma. In other words, the positive $\varepsilon_{Hf}(t)$ zircons would be crystallized from the magma that formed by either prompt reworking of juvenile crust or crustal contamination of mantle-derived magma, resulting in the "fictitiously" older depleted mantle model Hf ages of 0.94±0.06 to 1.18±0.06 Ga (Table 3). Therefore, it is important to identify the member of the coeval depleted mantle responsible for the juvenile crust (Zheng et al., 2006). Substantially, the juvenile source is only indicated by the highest positive $\varepsilon_{Hf}(t)$ values that are not only consistent with the values of the coeval depleted mantle but also associated with the single-stage model Hf ages identical to the zircon U–Pb ages for magma crystallization (Fig. 9).

If the end-member of ancient crust was also extracted from the depleted mantle at about 1.9 Ga with a $^{176}Lu/^{177}Hf$ ratio of 0.015, then the end-member of the

depleted mantle is assumed to evolve in the Lu–Hf isotope system since about 0.75 Ga (the line labeled "reworking of juvenile crust" in Fig. 9). However, the maximum $\varepsilon_{Hf}(t)$ values of 10.1 to 10.7 with the youngest T_{DM1} ages of 0.93 to 0.91 Ga occurs in gabbro KD111 from the Kangdian Rift (Table 1). This provides a constraint on the time for the addition of juvenile material to the crust. It would take place either by island-arc magmatism during the Rodinia assembly at 1.0 to 0.9 Ga (Wu et al., 2006a) or by crustal assimilation during the syn-rift magmatism at about 750 Ma (Zheng et al., 2006). No growth of juvenile crust is expected to occur along the Jiangnan Orogen during arc–continent collision magmatism at 900±20 Ma or post-collisional magmatism at ~825 Ma (Wu et al., 2006a). In this regard, those intrusives that have the T_{DM1} ages of about 0.2 to 0.4 Ga older than the timing of magma crystallization have certainly incorporated certain amounts of crustal component and thus would be brought about by rift magmatism. It is possible that the juvenile crust formed in the active rifting zone at about 760 to 750 Ma, but became promptly reworked at about 750 Ma with the considerable incorporation of supracrustal material into the magma sources via remelting of hydrothermally altered rocks. As a result, the bimodal magmatism of the second generation would be produced with the characteristic occurrence of low-^{18}O magmas and young model Hf ages along the active rifting zone.

6. Implications for growth and reworking of continental crust

With respect to timing and geometry of post-orogenic extension, two basic modes are orogenic collapse and continental rifting (Dewey, 1988; Ryan and Dewey, 1997). Because ancient collisional belts are favorite places for orogenic collapse, rift magmatism and continental breakup (Dewey, 1988; Vauchez et al., 1997; Tommasi and Vauchez, 2001), attributes of orogenic lithosphere are susceptible to reactivation by extensional tectonics and thermal anomalies. The continental rifting tends to follow weak zones in the lithosphere, such as arc–continent collision orogenic belts. These old tectonic belts not only influence the location of rifting, but also the inherited lithosphere architecture plays a role in the rifting process itself, the thermal evolution of the rift, and decompression melting of asthenospheric mantle and thus growth of juvenile crust during rifting (Zheng et al., 2006). On the other hand, the orogenic collapse can occur in arc–continent and continent–continent collision zones in response to post-collisional extension (Wu et al., 2006a; Xie et al., 2006). Once the orogenic collapse took place after the collision, however, collapsed orogens generally did not become the sites of opening of major oceans by the continental rifting. Reworking of juvenile and ancient crusts thus occurs by melting of orogenic lithospheric keel, resulting in intracrustal differentiation and thus shaping the chemical characteristics of continental crust (e.g., Zhao et al., 2005, 2007; Huang et al., 2006; Wu et al., 2006a).

While the zircon U–Pb age for igneous rocks represents the timing of magma crystallization, the single-stage model Hf age (T_{DM1}) with the positive $\varepsilon_{Hf}(t)$ value can be used as a proxy for the maximum age of magma extraction from the depleted mantle but the two-stage model Hf age (T_{DM2}) provides a first approximation to the source age of host magma from which the negative $\varepsilon_{Hf}(t)$ zircon crystallized. A close match between the U–Pb age and the T_{DM1} age with the highly positive $\varepsilon_{Hf}(t)$ values is clearly a signature for the growth and prompt reworking of juvenile crust during rift magmatism and thus for significant transport of both heat and material from the depleted mantle to the continental crust in this process. As exemplified by Zheng et al. (2006), two cases in point are protolith of orthogneiss from Port Morvan and Jospinet within the Cadomian Orogen in northwest France (Samson et al., 2003), and plagiogranite associated with the Tasriwine ophiolite from the Anti-Atlas orogen in Morocco (Samson et al., 2004).

For the orthogneiss in the Cadomian Orogen, Samson et al. (2003) carried out both U–Pb and Lu–Hf isotopic analyses of zircon. Bulk-grain zircon ID-TIMS U–Pb dating for the two localities of orthogneiss yielded $^{207}Pb/^{206}Pb$ ages of 754.6±0.8 Ma and 746.0±0.9 Ma, respectively, for their protolith. Lu–Hf isotope analyses gave highly positive $\varepsilon_{Hf}(t)$ values of 12.2±0.4 to 13.9±0.3 (recalculated using the decay constant for ^{176}Lu of 1.865×10^{-11} yr^{-1} from the original Lu–Hf data), with young T_{DM1} ages of 0.77±0.01 to 0.83±0.01 Ga that closely match the U–Pb ages of 746.0 to 754.6 Ma for magma emplacement (open triangles in Fig. 9). As concluded by Samson et al. (2003), a substantial input from the depleted mantle to the crust occurred during the mid-Neoproterozoic magmatism. For the plagiogranites in the Anti-Atlas orogen, Samson et al. (2004) also did such a combined study. While bulk-grain zircon ID-TIMS U–Pb dating for the two plagiogranite samples gave consistent discordia upper-intercept ages of 761±2 Ma and 762±2 Ma for the timing of magma crystallization, Lu–Hf isotope analyses yielded highly positive $\varepsilon_{Hf}(t)$ values of 14.0±0.3 to 14.9±0.6 with young T_{DM1}

ages of 0.74±0.02 to 0.77±0.01 Ga (open squares in Fig. 9). The good agreement between the zircon U–Pb and model Hf ages clearly points to the growth of juvenile crust from the depleted mantle and prompt reworking by the ca. 760 Ma magmatism (Zheng et al., 2006).

Similar to the interpretation to whole-rock Nd model ages (Arndt and Goldstein, 1987), however, caution is necessary when interpreting the $\varepsilon_{Hf}(t)$ values and model Hf ages for igneous zircons with respect to crust–mantle mixing. If a zircon has not only very positive $\varepsilon_{Hf}(t)$ values equivalent to those for coeval deplete mantle, but also single-stage model Hf ages coincidence with zircon U–Pb ages, an end-member of the depleted mantle is identified to occur in the zircon. In this case, crust–mantle differentiation can be assumed to result in the growth of juvenile crust with prompt reworking. Although a set of cogenetic samples may show large variations in both $\varepsilon_{Hf}(t)$ value and model Hf age, the identification of depleted-mantle end-member is critical for any model of crust–mantle mixing in igneous petrogenesis (Zhao et al., 2005; Zheng et al., 2006). If, on the other hand, negative $\varepsilon_{Hf}(t)$ values are obtained with the two-stage model Hf ages that coincide with relict zircon U–Pb ages, reworking of ancient crust is indicated without crust–mantle mixing. In many cases, however, a set of cogenetic samples show intermediate $\varepsilon_{Hf}(t)$ values that lie between those defined by the two end-members of mantle and crustal sources and also intermediate model Hf ages between groups of zircon U–Pb ages. This can result either from reworking of a heterogeneous source by anatexis, or from a binary mixing that may occur either between the depleted mantle and the ancient crust, or between two different ages of ancient crust. Because variation ranges for the initial Hf isotope ratio can be relatively narrowed by mixing, the model Hf ages represent an average age of this mixed source and thus do not date any specific event for crustal growth or reworking. Thus the positive $\varepsilon_{Hf}(t)$ values less than those for the coeval depleted mantle do not indicate extraction of the depleted mantle during magmatism. They are better interpreted as reworking of lithospheric keel by anatexis.

With respect to the Neoproterozoic intrusives in South China, geochemical investigation shows that the ~825 Ma granitoids in North Guangxi are exclusively peraluminous with A/CNK values of 1.01 to 1.31 (Li et al., 2003a), indicating that they were principally derived from remelting of supracrustal materials. The O isotope analyses in this study gave high $\delta^{18}O$ values of 8.7 to 10.4‰ for zircon from the granitoids (Table 3), demonstrating that the source material for felsic magmas was composed of rocks which had been through low-T alteration or surface chemical weathering processes to acquire their high $\delta^{18}O$ values before the remelting (Wu et al., 2006a). In this regard, the Guangxi granitoids were derived from the supracrustal rocks that were deeply buried in a contractional period before the magma generation in a subsequent extensional period. Thus they correspond to the S-type granite in the classification of Chappell and White (1974). Post-collisional extension may be the basic cause for orogenic collapse that results in this episode of S-type magmatism along the Jiangnan Orogen (Wu et al., 2006a). This episode of magmatism occurs extensively along the margins of the Yangtze Craton (Li, 1999; Li et al., 1999; Zhou et al., 2002a,b; Li et al., 2003a,b; Zhou et al., 2006; Wang et al., 2006; Wu et al., 2006a), possibly marking not only the final assembly between the Yangtze and Cathaysia Cratons but also the onset of rift tectonics along the arc–continent collisional Jiangnan Orogen.

The zircon Lu–Hf isotope analyses for the granitoids in the Jiangnan Orogen yield negative $\varepsilon_{Hf}(t)$ values of −3.4±0.8 to −1.6±0.8 with old model T_{DM2} ages of 1.81±0.07 to 1.92±0.10 Ga (Table 3). This observation is consistent with the whole-rock Sm–Nd isotope analyses that gave negative $\varepsilon_{Nd}(t)$ values of −9.0 to −3.9 for the Guangxi granitoids (Li et al., 2003a). There is also regional occurrence of 828±7 Ma diabase dykes (Li et al., 1999) with negative $\varepsilon_{Nd}(t)$ values of −4.2 to −3.4 (Ge et al., 2001) and high $\delta^{18}O$ values of 8.1 to 8.8‰ for quartz and plagioclase (Table 2). It is possible

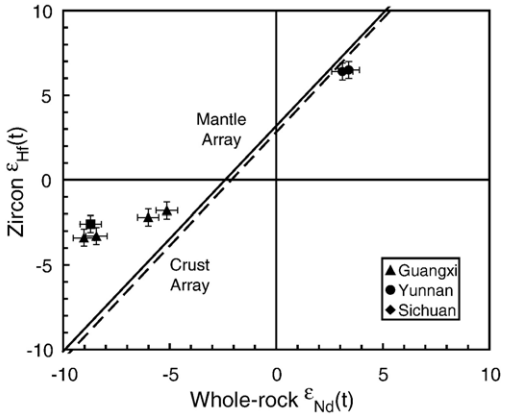

Fig. 10. Relationship between zircon Hf and whole-rock Nd isotopes for Neoproterozoic igneous rocks in South China (for data, refer to Table 3). Mantle array and crust array are referred to Vervoort et al. (1999). Decoupling of zircon Hf versus whole-rock Nd isotopes in S-type granitoids is interpreted as being due to the zircon effect: retention of radiogenic Hf in igneous zircons during chemical weathering and partial melting of ancient crust.

that protoliths of the bimodal intrusives at about 825 Ma were primarily extracted from the depleted mantle at about 2.0–1.8 Ga, but they had further evolved with the Hf–Nd isotope features of the enriched mantle at the time when the Neoproterozoic magmatism took place.

As illustrated in Fig. 10, the zircon $\varepsilon_{Hf}(t)$ values for the S-type granitoids are positively deviated from the whole-rock $\varepsilon_{Nd}(t)$ values with reference to the average arrays of mantle and crust Hf–Nd isotope evolution (Vervoort et al., 1999), suggesting somewhat Hf–Nd isotope decoupling. Abnormal enrichment of radiogenic Hf isotopes in crustal rocks is principally related to anomalously high Lu/Hf ratios in their magmatic source. Because garnet is a mineral rich in HREE, its presence or absence as a residual phase during partial melting strongly influences both concentrations and partitioning of Lu and Hf in extracted melts (i.e. garnet effect). This makes the Hf–Nd isotope decoupling sensitive to the role of garnet during intracrustal differentiation processes (e.g., Johnson et al., 1996; Vervoort et al., 2000; Schmitz et al., 2004). In general, the following two processes can result in the Hf–Nd isotope decoupling: (1) melt extraction in the presence of garnet to produce higher Lu/Hf ratios in a restite, (2) crystallization of garnet from magma to bring about high Lu/Hf ratios in a cumulate. Both processes can result in the preferential retention of Lu over Hf in the restite and thus HREE depletion in the melts. If the garnet did exist as a residue in the magma source, granitoids crystallized from evolved magmas show not only strong HREE depletion like those observed in adakites ($Yb \leq 1.8$ ppm, $Y \leq 18$ ppm; cf. Martin, 1999), but also a progressive decrease in HREE with atomic number. Although whole-rock REE analyses did exhibit HREE depletion relative to LREE in the S-type granitoids (Li, 1999; Li et al., 2003a), the HREE depletion is not strong enough to complement the crystallization of garnet in the source. Thus the presence of garnet can be ruled out as the residue in the magma source during partial melting.

Because zircon is a resistant and refractory mineral during chemical weathering and partial melting, it is capable of preserving its primary Hf isotope composition of magma crystallization. Following the arguments presented by Wu et al. (2006a), we explain the decoupling of zircon Hf versus whole-rock Nd isotopes in the S-type granitoids as being due to retention of radiogenic Hf in igneous zircons during chemical weathering and partial melting of ancient crust (i.e. zircon effect). It is suggested that zircon retains its Hf isotope signature acquired during crystallization from arc-derived magma, whereas the whole-rock Sm–Nd system was readily equilibrated with the new melt and hence gave the lower $\varepsilon_{Nd}(t)$ values. As a result, the granitoids have the less radiogenic Nd isotope compositions than the normal terrestrial rocks, but the zircons that crystallized from such an evolved source show the high $\varepsilon_{Hf}(t)$ ratios above the Hf–Nd terrestrial array (Fig. 10).

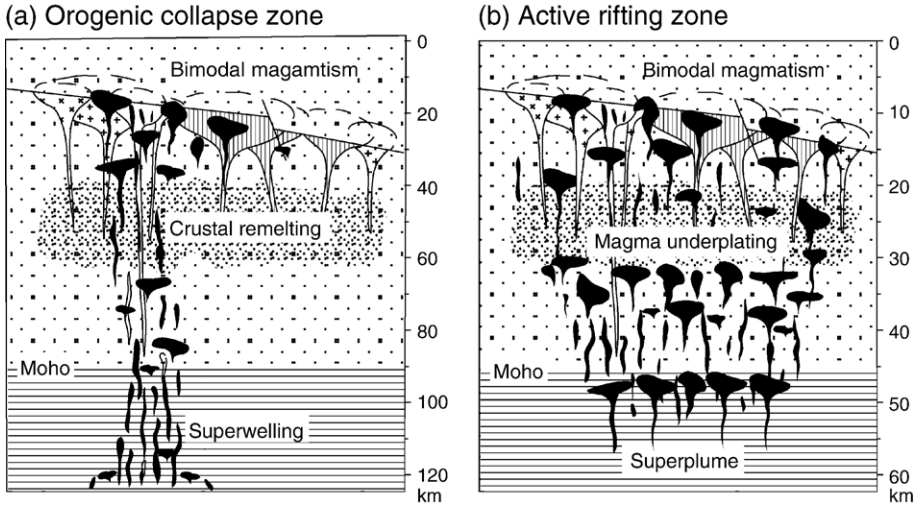

Fig. 11. Schematic diagrams for two episodes of bimodal magmatism along the margins of the Yangtze Craton during the middle Neoproterozoic. (a) The first phase magmatism at about 825 Ma was triggered by post-collisional orogenic collapse in combination with a thermal pulse due to mantle superwelling beneath the thickened lithosphere, resulting in reworking of ancient 2.0~1.8 Ga crust along the arc–continent belt; (b) the second phase magmatism at about 750 Ma proceeded by underplating of mafic magma derived from the asthenospheric mantle, with prompt reworking of juvenile crust via remelting of hydrothermally altered rocks along the active rifting zones.

Furthermore, melting of orogenic lithospheric keel is favored by an additional heat supply from asthenospheric upwelling to extensionally collapsed orogens (Thompson and Connolly, 1995). Hence a thermal pulse due to a mantle plume event could be assumed to cause the melting of collision-thickened orogens that encompasses both the enriched mantle and the buried sediments (Campbell and Hill, 1988; Kent et al., 1992), resulting in the granitoid magmatism of the first generation in the Jiangnan Orogen at ~825 Ma. This could just be a thermal response to orogenic collapse at that time (Dewey, 1988), with the additional effect of heat flux by mantle upwelling on the thickened lithosphere beneath preexisting orogenic belts (Hill et al., 1992; Hill, 1993).

The thickening of continental lithosphere generally takes place along the margin of convergent plates such as is observed in collision orogens of continent–continent (e.g., Himalaya: Liegeois et al., 1998; Variscan; Sylvester, 1998; Miditerranean: Dini et al., 2002; Dabie: Zhao et al., 2005, 2007; Sulu: Huang et al., 2006) and arc–continent (e.g., the Lachlan Fold Belt: Collins, 2002; Jiangnan Orogen: Wu et al., 2006a). Thus the generation of typical S-type granites is associated with the tectonic settings of post-collisional orogen. In this regard, the magmatism of early pre-rift association in South China took place along the preexisting orogenic belt (Fig. 11a). The magmatic history of generating the S-type granites could be explained by conductive heat transfer upward from the top of plume heads, if they did exist, that had presumably ascended to near the base of the crust (Hill et al., 1992). The O isotope analyses of mineral pairs from some of the pre-rift granitoids show the disequilibrium fractionations (Fig. 7), indicating the post-magmatic alteration by both internally derived and exotic fluids. The preservation of high $\delta^{18}O$ values for zircon demonstrates that the high-T water–rock interaction would take place under subsolidus conditions during magma emplacement at ~825 Ma, but it did not cause the low-^{18}O magmatism.

On the other hand, the ca. 760–750 Ma bimodal intrusives from West Sichuan are characterized by positive $\varepsilon_{Hf}(t)$ values of 3.5±0.8 to 9.9±0.8 with young T_{DM1} ages of 0.94±0.06 to 1.18±0.06 Ga (Table 3). Whole-rock Sm–Nd isotope analyses also yielded positive $\varepsilon_{Nd}(t)$ values of 0.9 to 3.4 for mafic dykes in the Kangdian Rift (Li et al., 2003b). The zircon $\varepsilon_{Hf}(t)$ and whole-rock $\varepsilon_{Nd}(t)$ values fall close to the array of crust Hf–Nd isotope evolution (Fig. 10), suggesting Hf–Nd isotope coupling with concordant incorporation of crustal Hf and Nd into their magma sources. Because the bimodal magmatism of the second generation exclusively occurred along the active rifting zone, the predominant contributions of the juvenile crust to their magma sources are evident in the rifted continental margin where the extensional thinning of lithosphere is the most significant during supercontinent breakup (Fig. 11b). Thus the large volumes of juvenile material were added to the crust along the active rifting zone at about 750 Ma when the South China Block was splitting from the supercontinent Rodinia (Zheng et al., 2006). This indicates not only higher-level underplating of mafic magmas in the matured stage of continental rift, but also the progressive effect of mantle upwelling on the overlying lithosphere during the superplume event (Hill, 1991; Kent et al., 1992), from the heat flux in the early phase to both heat and mass transfers in the late phase. The O isotope analyses of zircon show both low and high $\delta^{18}O$ values of 4.2 to 6.2‰ relative to 5.3±0.3‰ for the normal mantle zircon (Table 2), suggesting the formation of local low-^{18}O bimodal magmas in the active rifting zone. High LOI values of 2.2 to 7.8% were obtained in similar gabbro samples (Li et al., 2003b), indicating variable degrees of hydrothermal alteration. Zircons of 758±15 Ma ages with low $\delta^{18}O$ values are also observed for protoliths of bimodal metaigneous rocks along the northern margin of the Yangtze Craton (Zheng et al., 2004). Thus the large volumes of supracrustal fluid are associated with this episode of syn-rift magmatism via remelting of altered rocks.

Active rifting zones are known to favor high-T water–rock interaction and production of local ^{18}O depletion in magma source (Taylor, 1977, 1986). High heat from mantle upwelling may be responsible for the syn-rift magmatism that was capable of not only producing the bimodal igneous rocks with the geochemical feature of juvenile crust, but also causing the high-T supersolidus water–rock interaction and even low-^{18}O magmatism (Zheng et al., 2004, 2006). In comparison to the magmatism of the first generation at ~825 Ma, it appears that significant amounts of the depleted mantle material were transformed into the continental crust during the bimodal magmatism of the second generation at about 750 Ma and thus the juvenile crust was produced along the active rifting zones. The contemporaneous addition of both mantle-derived magma and surface fluid to the juvenile crust is associated with the extensional thinning of lithosphere. This also indicates the growth of continental crust by rift magmatism during the peak phase of supercontinent breakup (Zheng et al., 2006).

The ca. 825 magmas have high $\delta^{18}O$ values of 8.7 to 10.4‰ but low $\varepsilon_{Hf}(t)$ values of −3.4 to −1.6 with old model Hf ages of 1.92 to 1.81 Ga, whereas the ca. 760–750 magmas have relatively low $\delta^{18}O$ values of 4.2 to

6.2‰ but positive $\varepsilon_{Hf}(t)$ values of 3.5 to 9.9 with young model Hf ages of 1.18 to 0.94 Ga (Fig. 5). Thus the early melts occurred in the Paleoproterozoic basement that experienced the chemical weathering, whereas the late melts occurred at the high crustal levels with the prominent addition of juvenile materials along the rifted continental margin. Furthermore, arc–continent collision is suggested to occur in the early Neoproterozoic along the Jiangnan Orogen (Wang et al., 2006; Wu et al., 2006a), and Neoproterozoic igneous rocks along the western margin of the Yangtze Craton show both arc- and rift-like partition patterns of trace elements (Zhou et al., 2002a,b, 2006; Li et al., 2003b). Although mature rifts were developed along the western and northern margins of the Yangtze Craton (Li et al., 2003b; Zheng et al., 2006), the Neoproterozoic igneous rocks in the periphery of the Yangtze Craton may have a common evolution from oceanic subduction and oceanic/continental arc magmatism to arc–continent collision and melting of juvenile/ancient crust to post-collisional S-type magmatism in the pre-rift phase and syn-rift bimodal magmatism in association with supercontinent breakup. Nevertheless, the transport of energy and matter from the mantle to the crust is different for the different episodes of magmatism along the preexisting arc–continent collision belts.

It was advocated by some thermal plume models (Richards et al., 1989; Hill et al., 1992) that the arrival of a starting plume head beneath continental lithosphere serves as the driving force for the rifting of a supercontinent, thereby providing a single "plume origin" explanation for both continental breakup and rift magmatism. A mantle plume of ~825 Ma age was envisaged by Li et al. (1999) to trigger the Rodinia breakup in South China, and a mantle superplume event at about 830 to 740 Ma has been hypothesized by Li et al. (2003b) to initiate the Rodinia breakup and subsequent rift-magmatism worldwide. According to whole-rock geochemical studies and zircon U–Pb dating on Neoproterozoic igneous rocks in South China, the magmatism at ~825 Ma was interpreted by Li et al. (2003a) as products of the superplume event. However, this interpretation has been challenged and alternative models for island-arc or post-collisional origins have been proposed for this period of magmatism at different zones (Zhou et al., 2002a,b, 2004, 2006; Wang et al., 2004, 2006; Wu et al., 2006a). In this regard, a critical question regarding a proposed plume at any locality is where is the mantle plume? Indeed no actual material specifically related to a mantle plume has been identified so far in any of the ~825 Ma igneous rocks in South China.

Because the Yangtze and Cathaysia Cratons did not split up along the Jiangnan Orogen during the separation of the South China Block from the supercontinent Rodinia at ~750 Ma (Zheng et al., 2006), extensional collapse of the arc–continent collision orogen is suggested to cause burial and melting of evolved arc-derived sediments and underlying substrate at ~825 Ma (Wu et al., 2006a). The model of post-collisional collapse is also applicable to the contemporaneous S-type magmatism in the western part of the Jiangnan Orogen. Thickened lithospheric mélange of collision zones would easily undergo partial melting to produce melts with a similar crustal heritage. In this regard, the extensional collapse of the collision-thickened orogen along the southeastern margin of the Yangtze Craton can provide a geodynamic setting necessary to cause the S-type magmatism at ~825 Ma. The S-type granitoid magmas in the eastern part of the Jiangnan Orogen has been demonstrated to have major derivation from melting of juvenile crust in the early Neoproterozoic age (Wu et al., 2006a), whereas those in the western part of the Jiangnan Orogen appear to have major derivation from melting of ancient crust in the Paleoproterozoic age (this study). In this context, the former corresponds to reworking of oceanic arc crust whereas the latter to reworking of continental arc crust. In either case, a cyclical process took place during the early Neoproterozoic between the Cathaysia and Yangtze Cratons, including subduction of oceanic crust, arc magmatism, arc–continent collision and associated reworking of juvenile/ancient crust, uplift-erosion and sedimentation, post-collisional collapse and anatexis.

Although collapsed orogens are not a preferred site of continental rifting, a transformation of geotectonic framework from compressional to extensional regimes would take place at ~825 Ma in the South China Block (Wu et al., 2006a). A starting mantle plume rising from such a thermal boundary layer as the core–mantle boundary or the transition zone, would be generally characterized by a large mushroom-like head followed by a narrow conduit. The impact of plume heads as a superplume, if did exist, could nicely explain both the vast spatial extent (by the dimension of plume heads) and the large melt volume (by the high temperature of plume materials) of continental breakup magmatism during the middle Neoproterozoic in various parts of the supercontinent Rodinia. Essentially, the plume impact hypothesis is a theory that attributes anomalous mantle melting to thermal anomalies in convecting mantle. Thus it becomes controversial whether the disintegration of a supercontinent was principally controlled by the impingement of mantle superplume (Morgan, 1981;

Richards et al., 1989; Hill, 1991; Storey and Kyle, 1997; White, 1997) or by changes in plate boundary forces (Anderson, 1982; Le Pichon and Huchon, 1984; Cox, 1988; Storey et al., 1992). Basic questions have been how to identify the contribution of energy and matter from mantle plumes (or a superplume) in igneous petrogenesis and how to distinguish plume-related igneous rocks from those derived from island-arc magmatism or by anatexis of orogenic lithospheric keels. The present study provides a sound approach to identify the origin of mafic magmas derived from the asthenospheric mantle during the supercontinent breakup. As a result, it suggests that the hypothesized superplume may be originated from the thermal boundary layer at the top of the upper mantle rather than at the transition zone or the core–mantle boundary. In this regard, the nature of the Neoproterozoic superplume may resemble the mantle superwelling as defined by Larson (1991a,b) for the middle Cretaceous superplume.

Furthermore, the present study of zircon Hf and O isotopes provides the geochemical demonstration for the two episodes of crust–mantle interaction at ~825 Ma and ~750 Ma, respectively (Fig. 9). Along with the previous studies of Neoproterozoic igneous rocks in the other margins of the Yangtze Craton (Zheng et al., 2004, 2006; Wu et al., 2006a), the first episode of magmatism is characterized by the reworking of juvenile and ancient crusts along the arc–continent collision orogen, with the post-magmatic hydrothermal alteration. No plume-derived material has been found so far in this episode of igneous rocks. This only points to heat transfer from the mantle to the crust, with potential effect on the anatexis of orogenic lithospheric keel in combination with post-collisional extension collapse. The second episode of magmatism is characterized by the growth and prompt reworking of juvenile crust (or partial melting of juvenile lithospheric mantle to generate the juvenile crust) along the rifted continental margins, with supersolidus water–rock interaction and local low-^{18}O magmatism. Because the growth of juvenile crust did not occur in the first episode of magmatism (pre-rift), splitting of the South China Block from the supercontinent Rodinia did not commence at about 825 Ma. The growth of juvenile crust did occur in the second episode of magmatism (syn-rift), so that separation of the South China Block from the supercontinent Rodinia took place at about 750 Ma (Zheng et al., 2006). Furthermore, the change in melt source from the crust to the mantle is temporally associated with the advance from continental rifting to supercontinental breakup.

7. Conclusions

Two generations of mid-Neoproterozoic granitoids in South China show contrasting features of zircon Hf and O isotopes. Growth and reworking of continental crust are thus linked to supercontinent breakup, rift magmatism and orogenic collapse. In particular, igneous zircons crystallized from the promptly reworked juvenile crust not only have $\varepsilon_{Hf}(t)$ values close to the initial Hf isotope ratios of the contemporaneous depleted mantle, but also are associated with youngest model Hf ages close to extraction time of juvenile crust from mantle-derived magmas. Hence the reworking event of juvenile and ancient crusts is recovered from zircon $\varepsilon_{Hf}(t)$ values and model Hf ages in combination with U–Pb dates.

The first generation of pre-rift magmatism took place at ~825 Ma when post-collisional extension collapse occurred in combination with the mantle upwelling that heated the base of orogenic lithosphere keel, resulting in reworking of ancient (~2.0–1.8 Ga) crust and underlying lithospheric mantle to generate mafic to felsic igneous rocks that have the Hf isotope signatures of enriched mantle. High-*T* subsolidus alteration occurred during magma emplacement, but no low-^{18}O magmas formed as indicated by high zircon δ^{18}O values. With the development of syn-rift magmatism in association with the supercontinent breakup, the second generation of bimodal magmatism developed at ~750 Ma along active rifting zones. This not only gave rise to the bimodal igneous rocks that have the Hf isotope signatures of juvenile crust, but also brought about high-*T* supersolidus water–rock interaction and localized low-^{18}O magmatism as indicated by low zircon δ^{18}O values. Orogenic collapse in combination with the mantle upwelling results in the anatexis of orogenic lithospheric keel and the formation of rift basins on one hand, continental rifting gives rise to growth and prompt reworking of juvenile crust on the other hand. Both magmatic and sedimentary additions took place in a period of continental extension, with localized and repeated crustal reworking events along the rifted continental margins. Therefore, the orogenic collapse was developed for post-collisional S-type magmatism along the preexisting arc–continent collision orogenic belt before breakup of the supercontinent Rodinia at about 750 Ma.

The two generations of magmatism represent two episodes of crust–mantle interaction at ~825 and ~750 Ma, respectively, with different energy and matter contributions. The first episode is manifested only by heat supply beneath the collision-thickened orogen with post-magmatic alteration, whereas the second episode is

marked by the transport of both heat and material from the depleted mantle to the continental crust in the rifted continental margin. Therefore, the granitoid magmatism was episodically related to the continental rifting in the period of about 830 to 740 Ma along the margins of the Yangtze Craton. Although active rifting zones are favorable sites for both high-T hydrothermal alteration and low-^{18}O magmatism, our studies for the mid-Neoproterozoic intrusives in South China demonstrate that the post-magmatic alteration occurred during pre-rift magmatism in the post-collisional collapse phase, whereas the supersolidus water–rock interaction and low-^{18}O magmatism took place during the syn-rift magmatism in the peak phase of continental rifting. The extensional thinning of lithosphere is witnessed by the addition of both mantle-derived magma and supracrustal material to the juvenile crust during the supercontinent breakup, with localized and repeated water–rock interactions along matured rift tectonic zones. The transition from the anatexis of ancient crust at ~825 Ma to the growth and reworking of juvenile crust at ~750 Ma underlines the progressive transport of energy and matter between the mantle and the crust during orogenic collapse and continental rifting in association with the supercontinent breakup.

Acknowledgments

This study was supported by NSFC (40334036) and Chinese Academy of Sciences (KZCX3-SW-141). We thank Liewen Xie for assistance with LA-MC-ICPMS Hf isotope analysis. Comments by Y. Amelin, T. Andersen, A. Patchett, R. Stevenson, J. Woodhead and two anonymous reviewers helped for the improvement of the analytical data quality and the text presentation. Editorial handling by Yaoling Niu is also appreciated.

Appendix A. Supplementary data

Supplementary data associated with this article can be found, in the online version, at doi:10.1016/j.lithos.2006.10.003.

References

Albarede, F., 1998. The growth of continental crust. Tectonophysics 296, 1–14.

Anderson, D., 1982. Hotspots, polar wander, Mesozoic convection and the geoid. Nature 297, 391–393.

Arndt, N.T., Goldstein, S., 1987. Use and abuse of crust-formation ages. Geology 15, 893–895.

Belousova, E.A., Griffin, W.L., O'Reilly, S.Y., 2006. Zircon crystal morphology, trace element signatures and Hf isotope composition as a tool for petrogenetic modelling: examples from eastern Australian granitoids. J. Petrol. 47, 329–353.

Blichert-Toft, J., Albarede, F., 1997. The Lu–Hf geochemistry of chondrites and the evolution of the mantle–crust system. Earth Planet. Sci. Lett. 148, 243–258 (Erratum, 154, 349).

Brown, M., Rushmer, T., 2005. Evolution and Differentiation of the Continental Crust. Cambridge University Press, Cambridge.

Campbell, I.H., Hill, R.I., 1988. A two-stage model for the formation of the granite–greenstone terrains of the Kalgoorlie–Norseman area, Western Australia. Earth Planet. Sci. Lett. 90, 11–25.

Chappell, B.W., White, A.J.R., 1974. Two contrasting granite types. Pac. Geol. 8, 173–174.

Charvet, J., Shu, L.S., Shi, Y.S., Guo, L.Z., Faure, M., 1996. The building of south China: collision of Yangzi and Cathaysia blocks, problems and tentative answers. J. Southeast Asian Earth Sci. 13, 223–235.

Chu, N.C., Taylor, R.N., Chavagnac, V., Nesbitt, R.W., Boella, R.M., Milton, J.A., Germain, C.R., Bayon, G., Burton, K., 2002. Hf isotope ratio analysis using multi-collector inductively coupled plasma mass spectrometry: an evaluation of isobaric interference corrections. J. Anal. At. Spectrom. 17, 1567–1574.

Collins, W.J., 2002. Nature of extensional accretionary orogens. Tectonics 21 (4). doi:10.1029/2000TC001272.

Condie, K.C., 2000. Episodic continental growth models: afterthoughts and extensions. Tectonophysics 322, 153–162.

Condie, K.C., Chomiak, B., 1996. Continental accretion: Contrasting Mesozoic and Early Proterozoic tectonic regimes in North America. Tectonophysics 265, 101–126.

Corfu, F., Noble, S.R., 1992. Genesis of the southern Abitibi Greenstone belt, Superior Province, Canada: evidence from zircon Hf isotope analysis using a single filament technique. Geochim. Cosmochim. Acta 56, 2081–2097.

Corfu, F., Hanchar, J.M., Hoskin, P.W.O., Kinny, P., 2003. Atlas of zircon textures. Rev. Mineral. Geochem. 53, 469–500.

Courtillot, V., Davaille, A., Besse, J., Stock, J., 2003. Three distinct types of hotspots in the Earth's mantle. Earth Planet. Sci. Lett. 205, 295–308.

Cox, K.G., 1988. The Karoo province. In: Macdougall, J.D. (Ed.), Continental Flood Basalts. Kluwer Academic, Dordrecht, pp. 239–271.

Defant, M.J., Drummond, M.S., 1990. Derivation of some modern arc magmas by melting of young subducted lithosphere. Nature 347, 662–665.

Dewey, J.F., 1988. Extensional collapse of orogens. Tectonics 7, 1123–1139.

Dini, A., Westerman, D.S., Innocenti, F., Rocchi, S., Tonarini, S., 2002. The magmatic evolution of the late Miocene Laccolith–pluton–dyke granite complex of Elba Island Italy. Geol. Mag. 139, 257–279.

Ge, W.C., Li, X.H., Liang, X.R., Wang, R.C., Li, Z.X., Zhou, H.W., 2001. Geochemistry and geological implications of ~825 Ma mafic–ultramafic rocks in Yuanbaoshan–Baotan area of northern Guangxi. Geochimica 30, 123–130 (in Chinese with English abstract).

Giletti, B.J., 1986. Diffusion effects on oxygen isotope temperatures of slowly cooled igneous and metamorphic rocks. Earth Planet. Sci. Lett. 77, 218–228.

Griffin, W.L., Pearson, N.J., Belousova, E., Jackson, S.E., van Achterbergh, E., O'Reilly, S.Y., Shee, S.R., 2000. The Hf isotope composition of cratonic mantle: LAM-MC-ICPMS analysis of zircon megacrysts in kimberlites. Geochim. Cosmochim. Acta 64, 133–147.

Griffin, W.L., Wang, X., Jackson, S.E., Pearson, N.J., O'Reilly, S.Y., Xu, X., Zhou, X., 2002. Zircon chemistry and magma mixing, SE China: in-situ analysis of Hf isotopes, Tonglu and Pingtan igneous complexes. Lithos 61, 237–269.

Hanchar, J.M., Hoskin, P.W.O., 2003. Zircon. Rev. Mineral. Geochem. 16, 1–500.

Hawkesworth, C.J., Kemp, A.I.S., 2006. Using hafnium and oxygen isotopes in zircons to unravel the record of crustal evolution. Chem. Geol. 226, 144–162.

Hill, R.I., 1991. Starting plumes and continental break-up. Earth Planet. Sci. Lett. 104, 398–416.

Hill, R.I., Campbell, I.H., Davies, G.F., Griffiths, R.W., 1992. Mantle plumes and continental tectonics. Science 256, 186–193.

Hill, R.I., 1993. Mantle plumes and continental tectonics. Lithos 30, 193–206.

Hoskin, P.W.O., 2005. Trace-element composition of hydrothermal zircon and the alteration of Hadean zircon from the Jack Hills, Australia. Geochim. Cosmochim. Acta 69, 637–648.

Huang, J., Zheng, Y.-F., Zhao, Z.-F., Wu, Y.-B., Zhou, J.-B., Liu, X.M., 2006. Melting of subducted continent: element and isotopic evidence for a genetic relationship between Neoproterozoic and Mesozoic granitoids in the Sulu orogen. Chem. Geol. 229, 227–256.

Iizuka, T., Hirata, T., 2005. Improvements of precision and accuracy in in situ Hf isotope microanalysis of zircon using the laser ablation-MC-ICPMS technique. Chem. Geol. 220, 121–137.

Johnson, C.M., Shirey, S.B., Barovich, K.M., 1996. New approaches to crustal evolution studies and the origin of granitic rocks: what can the Lu–Hf and Re–Os isotope systems tell us? Trans. R. Soc. Edinb. Earth Sci. 87, 339–352.

Keay, S., Steele, D., Composton, W., 1999. Identifying granite sources by SHRIMP U–Pb zircon geochronology: an application to the Lachlan foldbelt. Contrib. Mineral. Petrol. 137, 323–341.

Kemp, A.I.S., Hawkesworth, C.J., Paterson, B.A., Kinny, P.D., 2006. Episodic growth of the Gondwana supercontinent from hafnium and oxygen isotopes in zircon. Nature 439, 580–583.

Kent, R.W., Storey, M., Saunders, A.D., 1992. Large igneous provinces: sites of plume impact or plume incubation? Geology 20, 891–894.

Larson, R.L., 1991a. Latest pulse of Earth: evidence for a mid-Cretaceous superplume. Geology 19, 547–550.

Larson, R.L., 1991b. Geological consequence of superplumes. Geology 19, 963–966.

Le Pichon, X., Huchon, P., 1984. Geoid, Pangea and convection. Earth Planet. Sci. Lett. 67, 123–135.

Liegeois, J.P., Black, R., Navez, J., Hertogen, J., 1998. Contrasting origin of post-collisional high calc-alkaline and shoshonitic versus alkaline and peralkaline granitoids: the use of sliding normalisation. Lithos 46, 1–28.

Li, X.-H., 1999. U–Pb zircon ages of granites from the southern margin of the Yangtze Block: timing of Neoproterozoic Jinning Orogeny in SE China and implications for Rodinia Assembly. Precambrian Res. 97, 43–57.

Li, Z.X., Li, X.-H., Kinny, P.D., Wang, J., 1999. The breakup of Rodinia: did it start with a mantle plume beneath South China? Earth Planet. Sci. Lett. 173, 171–181.

Li, Z.-X., Li, X.H., Zhou, H., Kinny, P.D., 2002a. Grenville-aged continental collision in South China: new SHRIMP U–Pb zircon results and implications for Rodinia configuration. Geology 30, 163–166.

Li, X.-H., Li, Z.-X., Zhou, H.-W., Liu, Y., Kinny, P.D., 2002b. U–Pb zircon geochronology, geochemistry and Nd isotopic study of Neoproterozoic bimodal volcanic rocks in the Kangdian Rift of South China: implications for the initial rifting of Rodinia. Precambrian Res. 113, 135–154.

Li, W.X., Li, X.H., 2003. Adakitic granites within the NE Jiangxi ophiolites, South China: geochemical and Nd isotopic evidence. Precambrian Res. 122, 29–44.

Li, X.-H., Li, Z.X., Ge, W., Li, W.-X., Liu, Y., Wingate, M.T.D., 2003a. Neoproterozoic granitoids in South China: crustal melting above a mantle plume at ca. 825 Ma? Precambrian Res. 122, 45–83.

Li, Z.X., Li, X.-H., Kinny, P.D., Wang, J., Zhang, S.-H., Zhou, H., 2003b. Geochronology of Neoproterozoic syn-rift magmatism in the Yangtze craton, South China and correlations with other continents: evidence for a mantle superplume that broke up Rodinia. Precambrian Res. 122, 85–109.

Machado, N., Simonetti, A., 2001. U–Pb dating and Hf isotopic composition of zircons by laser ablation-MC-ICP-MS. In: Sylvester, P. (Ed.), Laser-Ablation-ICPMS in the Earth Sciences: Principles and Applications. Short Course of Mineral. Assoc. Canada, vol. 29, pp. 121–146.

Martin, H., 1999. Adakitic magmas: modern analogues to Archean granitoids. Lithos 46, 411–429.

Morgan, W.J., 1981. Hotspot tracks and the opening of the Atlantic and Indian Oceans. In: Emiliani, C. (Ed.), The Sea. Wiley, New York, pp. 443–487.

Nowell, G.M., Kempton, P.D., Noble, S.R., Fitton, J.G., Saunders, A.D., Mahoney, J.J., Taylor, R.N., 1998. High precision Hf isotope measurements of MORB and OIB by thermal ionisation mass spectrometry: insights into the depleted mantle. Chem. Geol. 149, 211–233.

Richards, M.A., Duncan, R.A., Courtillot, V.E., 1989. Flood basalts and hot-spot tracks: plume heads and tails. Science 246, 103–107.

Rudnick, R.L., 1995. Making Continental Crust. Nature 378, 571–578.

Ryan, P.D., Dewey, J.F., 1997. Continental eclogites and the Wilson Cycle. J. Geol. Soc. (Lond.) 154, 437–442.

Samson, S.D., D'Lemos, R.S., Blichert-Toft, J., Vervoort, J., 2003. U–Pb geochronology and Hf–Nd isotope compositions of the oldest Neoproterozoic crust within the Cadomian orogen: new evidence for a unique juvenile terrane. Earth Planet. Sci. Lett. 208, 165–180.

Samson, S.D., Inglis, J.D., D'Lemos, R.S., Admou, H., Blichert-Toft, J., Hefferan, K., 2004. Geochronological, geochemical, and Hf–Nd isotopic constraints on the origin of Neoproterozoic plagiogranites in the Tasriwine ophiolite, Anti-Atlas orogen, Morocco. Precambrian Res. 135, 133–147.

Scherer, E., Munker, C., Mezger, K., 2001. Calibration of the lutetium–hafnium clock. Science 293, 683–687.

Schmitz, M.D., Vervoort, J.D., Bowring, S.A., Patchett, P.J., 2004. Decoupling of the Lu–Hf and Sm–Nd isotope systems during the evolution of granulitic lower crust beneath southern Africa. Geology 32, 405–408.

Sharp, Z.D., 1990. A laser-based microanalytical method for the in situ determination of oxygen isotope ratios of silicates and oxides. Geochim. Cosmochim. Acta 54, 1353–1357.

Storey, B.C., Alabaster, T., Hole, M.J., Pankhurst, R.J., Wever, H.E., 1992. Role of subduction–plate boundary forces during the initial stages of Gondwana break-up: evidence from the proto-Pacific margin of Antarctica. In: Storey, B.C., Alabaster, T., Pankhurst, R.J. (Eds.), Magmatism and the Causes of Continental Break-up. Spec. Pub. Geol. Soc., vol. 68, pp. 149–164.

Storey, B.C., Kyle, P.R., 1997. An active mantle mechanism for Gondwana breakup. S. Afr. J. Geol. 100, 283–290.

Sylvester, P.J., 1998. Post-collisional strongly peraluminous granites. Lithos 45, 29–44.

Taylor Jr., H.P., 1977. Water/rock interactions and the origin of H_2O in granitic batholiths. J. Geol. Soc. (Lond.) 133, 509–558.

Taylor Jr., H.P., 1986. Igneous rocks: II. Isotopic case studies of circumpacific magmatism. Rev. Mineral. 16, 273–317.
Thompson, A.B., Connolly, J.A.D., 1995. Melting of the continental crust: some thermal and petrologic constraints on anatexis in continental collision zones and other tectonic settings. J. Geophys. Res. 100, 15565–15579.
Tommasi, A., Vauchez, A., 2001. Continental rifting parallel to ancient collisional belts: an effect of the mechanical anisotropy of the lithospheric mantle. Earth Planet. Sci. Lett. 185, 199–210.
Valley, J.W., Chiarenzelli, J., McLelland, J.M., 1994. Oxygen isotope geochemistry of zircon. Earth Planet. Sci. Lett. 126, 187–206.
Valley, J.W., Kitchen, N., Kohn, M.J., Niendorf, C.R., Spicuzza, M.J., 1995. UWG-2, a garnet standard for oxygen isotope ratio: strategies for high precision and accuracy with laser heating. Geochim. Cosmochim. Acta 59, 5223–5231.
Valley, J.W., Kinny, P.D., Schulze, D.J., Spicuzza, M.J., 1998. Zircon megacrysts from kimberlite: oxygen isotope variability among mantle melts. Contrib. Mineral. Petrol. 133, 1–11.
Valley, J.W., 2003. Oxygen isotopes in zircon. Rev. Mineral. Geochem. 53, 343–385.
Vauchez, A., Barruol, G., Tommasi, A., 1997. Why do continents break-up parallel to ancient orogenic belts? Terra Nova 9, 62–66.
Vervoort, J.D., Blichert-Toft, J., 1999. Evolution of the depleted mantle: Hf isotope evidence from juvenile rocks through time. Geochim. Cosmochim. Acta 63, 533–556.
Vervoort, J.D., Patchett, P.J., Blichert-Toft, J., Albarede, F., 1999. Relationship between Lu–Hf and Sm–Nd isotopic systems in the global sedimentary system. Earth Planet. Sci. Lett. 168, 79–99.
Vervoort, J.D., Patchett, J.P., Albarede, F., Blichert-Toft, J., Rudnick, R., Downes, H., 2000. Hf–Nd isotopic evolution of the lower crust. Earth Planet. Sci. Lett. 181, 115–119.
Wang, J., Li, Z.-X., 2003. History of Neoproterozoic rift basins in South China: implications for Rodinia break-up. Precambrian Res. 122, 141–158.
Wang, X.L., Zhou, J.C., Qiu, J.S., Gao, J.F., 2004. Geochemistry of the Meso- to Neoproterozoic basic-acid rocks from Hunan Province, South China: implications for the evolution of the western Jiangnan orogen. Precambrian Res. 135, 79–103.
Wang, X.-L., Zhou, J.-C., Qiu, J.-S., Zhang, W.-L., Liu, X.-M., Zhang, G.-L., 2006. LA-ICP-MS U–Pb zircon geochronology of the Neoproterozoic igneous rocks from Northern Guangxi, South China: implications for tectonic evolution. Precambrian Res. 145, 111–130.
Watson, E.B., 1996. Dissolution, growth and survival of zircons during crustal fusion: kinetic principles, geological models and implications for isotopic inheritance. Trans. R. Soc. Edinb. Earth sci. 87, 43–56.
White, R.S., 1997. Mantle plume origin for the Karoo and Ventersdorp flood basalts, South Africa. S. Afr. J. Geol. 100, 271–282.
Williams, I.S., 1992. Some observations on the use of zircon U–Pb geochronology in the study of granitic rocks. Trans. R. Soc. Edinb. Earth Sci. 83, 447–458.
Woodhead, J., Hergt, J., Shelley, M., Eggins, S., Kemp, R., 2004. Zircon Hf-isotope analysis with an excimer laser, depth profiling, ablation of complex geometries, and concomitant age estimation. Chem. Geol. 209, 121–135.
Wu, R.-X., Zheng, Y.-F., Wu, Y.-B., Zhao, Z.-F., Zhang, S.-B., Liu, X.M., Wu, F.-Y., 2006a. Reworking of juvenile crust: element and isotope evidence from Neoproterozoic granodiorite in South China. Precambrian Res. 146, 179–212.
Wu, F.-Y., Yang, Y.H., Xie, L.W., Yang, J.H., Xu, P., 2006b. Hf isotopic compositions of the standard zircons and baddeleyites used in U–Pb geochronology. Chem. Geol. 234, 105–126. doi:10.1016/j.chemgeo.2006.05.003.
Xie, Z., Zheng, Y.-F., Zhao, Z.-F., Wu, Y.-B., Wang, Z.R., Chen, J.F., Liu, X.M., Wu, F.-Y., 2006. Mineral isotope evidence for the contemporaneous process of Mesozoic granite emplacement and gneiss metamorphism in the Dabie orogen. Chem. Geol. 231, 214–235.
Xu, P., Wu, F.-y., Xie, L.-w., Yang, Y.-h., 2004. Hf isotopic compositions of the standard zircons for U–Pb dating. Chin. Sci. Bull. 49, 1642–1648.
Yogodzinski, G.M., Lees, J.M., Churikova, T.G., Dorendorf, F., Woerner, G., Volynets, O.N., 2001. Geochemical evidence for the melting of subducting oceanic lithosphere at plate edges. Nature 409, 500–504.
Zhang, S.-B., Zheng, Y.-F., Wu, Y.-B., Zhao, Z.-F., Gao, S., Wu, F.-Y., 2006. Zircon isotope evidence for ≥3.5 Ga continental crust in the Yangtze craton of China. Precambrian Res. 146, 16–34.
Zhao, G.-C., Cawood, P.A. 1999. Tectonothermal evolution of the Mayuan assemblage in the Cathaysia Block: implications for Neoproterozoic collision-related assembly of the South China craton. Am. J. Sci. 299, 309–339.
Zhao, Z.-F., Zheng, Y.-F., Wei, C.-S., Gong, B., 2004a. Temporal relationship between granite cooling and hydrothermal uranium mineralization at Dalongshan in China: a combined radiometric and oxygen isotopic study. Ore Geol. Rev. 25, 221–236.
Zhao, Z.-F., Zheng, Y.-F., Wei, C.-S., Wu, Y.-B., 2004b. Zircon isotope evidence for recycling of subducted continental crust in post-collisional granitoids from the Dabie terrane in China. Geophys. Res. Lett. 31, L22602. doi:10.1029/2004GL021061.
Zhao, Z.-F., Zheng, Y.-F., Wei, C.-S., Wu, Y.-B., Chen, F.-K., Jahn, B.-m., 2005. Zircon U–Pb age, element and C–O isotope geochemistry of post-collisional mafic–ultramafic rocks from the Dabie orogen in east-central China. Lithos 83, 1–28.
Zhao, Z.-F., Zheng, Y.-F., Wei, C.-S., Wu, Y.-B., 2007. Post-collisional granitoids from the Dabie orogen in China: Zircon U–Pb age, element and O isotope evidence for recycling of subducted continental crust. Lithos 93, 248–272.
Zheng, Y.-F., 1991. Calculations of oxygen isotope fraction in metal oxides. Geochim. Cosmochim. Acta 55, 2299–2307.
Zheng, Y.-F., 1993a. Calculation of oxygen isotope fractionation in anhydrous silicate minerals. Geochim. Cosmochim. Acta 57, 107–1091.
Zheng, Y.-F., 1993b. Calculation of oxygen isotope fractionation in hydroxyl-bearing silicate. Earth Planet. Sci. Lett. 120, 247–263.
Zheng, Y.-F., Fu, B., 1998. Estimation of oxygen diffusivity from anion porosity in minerals. Geochem. J. 32, 71–89.
Zheng, Y.-F., Wang, Z.-R., Li, S.-G., Zhao, Z.-F., 2002. Oxygen isotope equilibrium between eclogite minerals and its constraints on mineral Sm–Nd chronometer. Geochim. Cosmochim. Acta 66, 625–634.
Zheng, Y.-F., Wu, Y.-B., Chen, F.-K., Gong, B., Li, L., Zhao, Z.-F., 2004. Zircon U–Pb and oxygen isotope evidence for a large-scale ^{18}O depletion event in igneous rocks during the Neoproterozoic. Geochim. Cosmochim. Acta 68, 4145–4165.
Zheng, Y.-F., Wu, Y.-B., Zhao, Z.-F., Zhang, S.-B., Xu, P., Wu, F.-Y., 2005. Metamorphic effect on zircon Lu–Hf and U–Pb isotope systems in ultrahigh-pressure eclogite-facies metagranite and metabasite. Earth Planet. Sci. Lett. 240, 378–400.
Zheng, Y.-F., Zhao, Z.-F., Wu, Y.-B., Zhang, S.-B., Liu, X.M., Wu, F.-Y., 2006. Zircon U–Pb age, Hf and O isotope constraints on protolith origin of ultrahigh-pressure eclogite and gneiss in the Dabie orogen. Chem. Geol. 231, 135–158.

Zhou, M.F., Yan, D.-P., Kennedy, A.K., Li, Y.-Q., Ding, J., 2002a. SHRIMP U–Pb zircon geochronological and geochemical evidence for Neoproterozoic arc-magmatism along the western margin of the Yangtze Block, South China. Earth Planet. Sci. Lett. 196, 51–67.

Zhou, M.F., Kennedy, A.K., Sun, M., Malpas, J., Lesher, C.M., 2002b. Neoproterozoic arc-related mafic intrusions along the northern margin of South China: implications for the accretion of Rodinia. J. Geol. 110, 611–618.

Zhou, J.C., Wang, X.L., Qiu, J.S., Gao, J.F., 2004. Geochemistry of Meso- and Neoproterozoic mafic–ultramafic rocks from northern Guangxi, China: arc or plume magmatism? Geochem. J. 38, 139–152.

Zhou, M.-F., Ma, Y.X., Yan, D.-P., Xia, X.P., Zhao, J.-H., Sun, M., 2006. The Yanbian Terrane (Southern Sichuan Province, SW China): a Neoproterozoic arc assemblage in the western margin of the Yangtze Block. Precambrian Res. 144, 19–38.